Translational Oncology
www.transonc.com

Volume 6 Number 2 April 2013 pp. 143–157 143

Endoplasmic Reticulum Stress Plays a Pivotal Role in Cell Death Mediated by the Pan-Deacetylase Inhibitor Panobinostat in Human Hepatocellular Cancer Cells[1,2]

Roberta Montalbano*, Petra Waldegger*, Karl Quint*, Samir Jabari†, Daniel Neureiter‡, Romana Illig‡, Matthias Ocker* and Pietro Di Fazio*

*Institute for Surgical Research, Philipps University of Marburg, Marburg, Germany; †Institute for Anatomy I, University of Erlangen-Nuremberg, Erlangen, Germany; ‡Institute of Pathology, Paracelsus Private Medical University, Salzburg, Austria

Abstract

Panobinostat, a pan-deacetylase inhibitor, represents a novel therapeutic option for cancer diseases. Besides its ability to block histone deacetylases (HDACs) by promoting histone hyperacetylation, panobinostat interferes with several cell death pathways providing a potential efficacy against tumors. We have previously demonstrated that panobinostat has a potent apoptotic activity *in vitro* and causes a significant growth delay of hepatocellular carcinoma (HCC) tumor xenografts in nude mice models. Here, we show that treatment with panobinostat is able to induce noncanonical apoptotic cell death in HepG2 and in Hep3B cells, involving the endoplasmic reticulum (ER) stress by up-regulation of the molecular chaperone binding immunoglobulin protein/glucose-regulated protein 78, activation of eukaryotic initiation factor 2α–activating transcription factor 4 (tax-responsive enhancer element B67) and inositol requiring 1α–X-box binding protein 1 factors, strong increase and nuclear translocation of the transcription factor C/EBP homologous protein/growth arrest and DNA damage–inducible gene 153, and involvement of c-Jun N-terminal kinase. These signaling cascades culminate into the activation of the ER-located caspase-4/12 and of executioner caspases, which finally lead to cell demise. Our results clearly show that panobinostat induces an alternative ER stress–mediated cell death pathway in HCC cells, independent of the p53 status.

Translational Oncology (2013) 6, 143–157

Introduction

Hepatocellular carcinoma (HCC) represents one of the most common malignancies worldwide and its treatment options still remain limited, especially in patients with compromised liver function. A multitude of different signaling pathways is altered in liver cancer cells and dysregulation of the balance between proliferation and cell death contributes to hepatocarcinogenesis [1].

Deacetylase inhibitors (DACis), a novel class of compounds, have shown strong antitumor activity in preclinical studies and are currently investigated in clinical trials for treatment of several blood and solid malignancies [2]. These compounds are able to induce cell death, cell differentiation, and/or cell cycle arrest in many different cancer models, through inhibition of enzymes involved in deacetylation of histones and other proteins, which promotes the re-expression of tumor suppressor genes [3].

Recent reports suggest that DACis can also induce accumulation of misfolded proteins and trigger endoplasmic reticulum (ER) stress–induced cell death in tumor cells by interfering with nonhistone proteins [4–7]. In particular, it has been shown that vorinostat (SAHA) is able to activate atypical ER stress–related apoptosis, acting as ER

Address all correspondence to: Dr Roberta Montalbano, PhD, Institute for Surgical Research, Philipps University of Marburg, Baldingerstrasse, 35043 Marburg, Germany. E-mail: montalba@med.uni-marburg.de

[1]The project was supported by a grant from Novartis Pharma GmbH (Nuremberg, Germany) and a research grant from the University Medical Center Giessen and Marburg (UKGM) to M.O. R.M. was supported by the von Behring-Roentgen Foundation (Marburg, Germany); P.D.F. was supported by a Sheila Sherlock Post Doc Fellowship from the European Association for the Study of the Liver. The authors P.W., K.Q., S.J., D.N., and R.I. declare no conflicts of interest.

[2]This article refers to supplementary materials, which are designated by Figures W1 to W4 and are available online at www.transonc.com.

Received 20 August 2012; Revised 1 February 2013; Accepted 4 February 2013

1944-7124/13/ DOI 10.1593/tlo.12271

stress mediator and apoptosis enhancer in oral squamous cell carcinoma and brain and prostate cancer models [6,7].

Panobinostat (LBH589), a cinnamic hydroxamic acid, is a novel pan-DACi that has shown potent antitumor activity in preclinical models and clinical trials [2,3,8,9].

We have previously demonstrated that panobinostat treatment was able to block cell proliferation in human HCC cell lines and to induce DNA damage and cell death *in vitro* and in subcutaneous xenograft models, independent of canonical intrinsic and/or extrinsic apoptotic pathways, which was probably mediated by alternative death mechanisms, like ER stress–induced apoptosis [10].

ER stress is a highly conserved cellular defense mechanism that responds to perturbations of ER function [11,12]. Factors that alter ER homeostasis, e.g., massive increase of protein synthesis, alteration of protein maturation mechanisms, decreased chaperone function, and alterations in calcium stores in the ER lumen, contribute to ER stress, resulting in a massive accumulation of unfolded/misfolded proteins [4,13,14].

As an initial response to ER stress, cells activate a cascade of recovery actions, named collectively unfolded protein response (UPR), that communicate information about protein-folding status to the nucleus, giving a prompt response to raise protein folding capacity, degrade misfolded proteins, and decrease *de novo* protein synthesis [14,15]. UPR is mediated by three distinct signaling pathways initiated by the ER-transmembrane transducers inositol requiring 1α (IRE1α), PKR-like ER kinase (PERK), and activating transcription factor (ATF) 6α [14–16], which are maintained in an inactive state through association with the ER chaperone binding immunoglobulin protein (BiP) in resting cells. Due to massive prolonged or unresolved ER stress, the accumulation of unfolded proteins leads to BiP dissociation and activation of the three ER stress sensors, triggering the UPR, a prosurvival cellular response that aims to reduce the huge mass of unfolded proteins and to overcome the effects of ER stress [17]. However, if the stress cannot be resolved, this adaptive process switches to a proapoptotic response, leading to elimination of cells unable to handle the unfolded protein accumulation through the UPR intervention [17–19].

The complete mechanisms promoting ER stress–induced cell death still remain unclear. However, it has been demonstrated that several other apoptosis mediators, like the transcription factor C/EBP homologous protein (CHOP), the mitogen-activated protein kinase c-Jun N-terminal kinase (JNK), and B-cell lymphoma 2 (Bcl-2) family proteins, are involved in ER stress–associated cell death and activated through the above-mentioned upstream factors [15,18]. The activation of these factors can promote the expression of cell death–related genes and/or modulate the activation of ER stress–sensible executioner caspases, like caspase-4/12, leading to apoptotic cell death.

Here, we investigate the ability of the pan-DACi panobinostat to activate ER stress–related apoptotic cell death in HCC cell lines, supporting the impact of alternative cell death pathways as potential new targets for cancer therapy and confirming the use of this compound as a promising anticancer drug.

Materials and Methods

Cell Culture and Reagents

Human HCC cell lines HepG2 (TP53wt) and Hep3B (TP53null) were cultured under standard conditions as previously described [10]. Cells were treated with 0.1 μM panobinostat (LBH589) and analyzed or processed for further experiments from 6 to 72 hours. Panobinostat was kindly provided by Novartis Pharma AG (Basel, Switzerland) and prepared as previously described [10]. Thapsigargin and SP600125 were purchased from Sigma-Aldrich (Munich, Germany) and dissolved in DMSO (Sigma-Aldrich).

Quantitative and Semiquantitative Reverse Transcription–Polymerase Chain Reaction

For semiquantitative polymerase chain reaction (PCR) and quantitative real-time PCR, total cellular RNA was extracted using the RNeasy Mini Kit (Qiagen, Hilden, Germany) according to the manufacturer's instructions and reverse transcription (RT) was performed with Quantitect Reverse Transcription Kit (Qiagen). For semiquantitative PCR, the Ready Mix Taq PCR Kit (Sigma-Aldrich) was used. The oligonucleotides 5′-CCTTGTAGTTGAGAACCAGG-3′ and 5′-GGGGCTTGGTATATATGTGG-3′ (Eurofins MWG Operon, Ebersberg, Germany) were used for amplification of the X-box binding protein 1 (XBP-1) transcript fragments. PCR products were resolved on two different 2% agarose gels, stained with Sybersafe DNA gel stain (Life Technologies, Darmstadt, Germany) and visualized under ultraviolet illumination using Fusion image capture (PEQLAB Biotechnologie GmbH, Erlangen, Germany). Glyceraldehyde-3-phosphate dehydrogenase (GAPDH) was amplified as an internal control.

For quantitative real-time PCR, QuantiTect Primers for IRE1α, IRE1β, BiP, ATF4, CHOP, and GAPDH were purchased from Qiagen and run with the QuantiFast SYBR Green PCR Kit (Qiagen) on a CFX96 Real-Time PCR Detection System (Bio-Rad, Munich, Germany). Results were analyzed with the CFX Manager v2.0 and Rest 2008 software and normalized to GAPDH mRNA content for each sample.

CHOP Transcript Modulation

siRNAs against CHOP Hs_DDIT3_1, _2, _3, and _5 were purchased from Qiagen. Transfection was performed with HiPerfect (Qiagen) following the Qiagen Fast Transfection Protocol as described by the company. Hs_DDIT3_1 siRNA showed the best transfection efficiency in both HCC cell lines and it was used for the following experiments. AllStars Negative Control (Qiagen) oligonucleotide was used as nonsilencing control.

Real-time Cell Viability Analysis

The xCELLigence RTCA SP System (Roche Applied Science, Mannheim, Germany) was used for real-time analysis of the cellular response of HepG2 and Hep3B cells following incubation with 0.1 μM panobinostat and SP600125 (100 nM and 10 μM) and transfection with CHOP siRNA as previously described [20]. Cell index, indicating attachment and adherence of cells to the plate's electrode, was measured for the following 70 hours continuously. Data analysis was performed using the RTCA Software v1.2.1.

Immunofluorescence

HepG2 and Hep3B cells were seeded in chamber slides (Lab Tek distributed by Fisher Scientific GmbH, Schwerte, Germany) and treated with 0.1 μM panobinostat and 10 nM thapsigargin for 24 and 48 hours. Immunofluorescence was performed as previously described [20]. Primary antibodies against BiP, ATF4, IRE1α, S724-IRE1α, and CHOP

were purchased from Abcam (Cambridge, United Kingdom) and secondary Alexa Fluor 488– and 568–conjugated antibodies from Life Technologies. The fluorescence was visualized with a Nikon microscope at ×630 magnification and acquired with a Hamamatsu ORCA-ER camera (model C4742-80) under the same setting. Obtained data were analyzed with ImageJ software v 1.43u. The quantification of the fluorescence signals was performed using the image processing software Photoshop from Adobe with the background-corrected fluorescence methods as described before [21].

Protein Extraction and Western Blot Analysis

Whole-cell lysates were obtained from HepG2 and Hep3B cell lines with or without treatment with panobinostat after 6 to 72 hours, and 10 nM thapsigargin after 24 hours, and further processed by sodium dodecyl sulfate–polyacrylamide gel electrophoresis followed by Western blot analysis, as previously described [20]. Immunodetection was performed with primary antibodies against BiP, eukaryotic initiation factor 2α (eIF2α), S51-eIF2α (Abcam), and β-actin (Sigma-Aldrich). Secondary HRP-conjugated antibodies (Sigma-Aldrich) were detected by incubating the immunoblots with SuperSignal West Pico Chemiluminescent Substrate (Pierce, Thermo Fisher Scientific). The luminescent reactivity was measured by using Fusion image capture and further quantified with Bio1D Analysis System (PEQLAB Biotechnologie GmbH). Anti–β-actin was used to control equal loading and protein quality.

Caspase Activity Assays

Caspase activity assays were performed as previously described [10] using Caspase Glo-8 and Caspase Glo-3/7 Luminescent Assays (both from Promega GmbH, Mannheim, Germany) or Caspase-12 and Caspase-4 Fluorometric Assay Kits (Biovision, Mountain View, CA) according to the manufacturer's protocol and GloMax 96 Microplate Luminometer (Promega) and Tecan GENios fluorometer (GENios; Tecan Germany GmbH, Crailsheim, Germany). All data were normalized to untreated controls. Cells were treated with 4 μM caspase-12 inhibitor Z-ATAD-FMK (BioVision) and caspase-4 inhibitor Z-LEVD-FMK (BioVision) for 48 hours to inhibit caspase activity.

Analysis of Apoptosis

Flow cytometry was employed for the quantification of apoptosis in treated cell lines after staining with propidium iodide as described previously [10]. Analysis of labeled nuclei was performed on an Attune acoustic focusing cytometer (Applied Biosystems, Carlsbad, CA) and results were analyzed with the Attune Cytometric Software 1.2.5.3891. All experiments were performed in triplicates. The percentage of apoptotic cells was determined by measuring the fraction of nuclei with a subdiploid DNA content. Ten thousand events were collected for each sample.

Sample Processing for Transmission Electron Microscopy

HepG2 and Hep3B cells were treated with panobinostat for 48 hours. Control and treated cells were harvested, centrifuged at 1000 rpm for 10 minutes at 4°C, and washed twice with Ca^{2+}/Mg^{2+}-free phosphate-buffered saline. Cell pellet was suspended in 2.5% glutaraldehyde 100 mM phosphate buffer (Sörensen's buffer), incubated for 90 minutes at 4°C, and then centrifuged at 1000 rpm for 10 minutes at 4°C. The pellet was washed twice with Sörensen's buffer and then suspended in the same buffer and kept at room temperature for 7 days. Cell pellet was post-fixed in Sörensen's buffer for 6 hours at

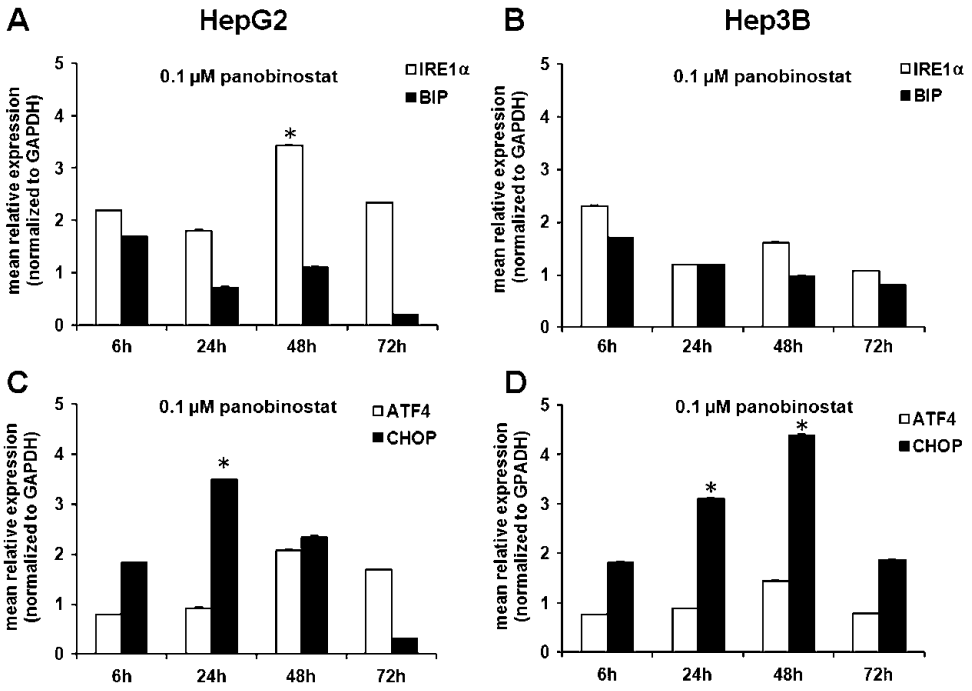

Figure 1. mRNA expression of ER stress–related factors. Quantitative RT-PCR analysis after 6, 24, 48, and 72 hours of treatment with 0.1 μM panobinostat in HepG2 (A and C) and Hep3B (B and D) cells showing an increase of IRE1α, BiP, ATF4, and CHOP. mRNA expression was normalized to GAPDH and results are expressed relative to untreated controls set at 1.0. Means ± SD of three independent experiments performed in triplicates are shown. *$P < .05$ *versus* control.

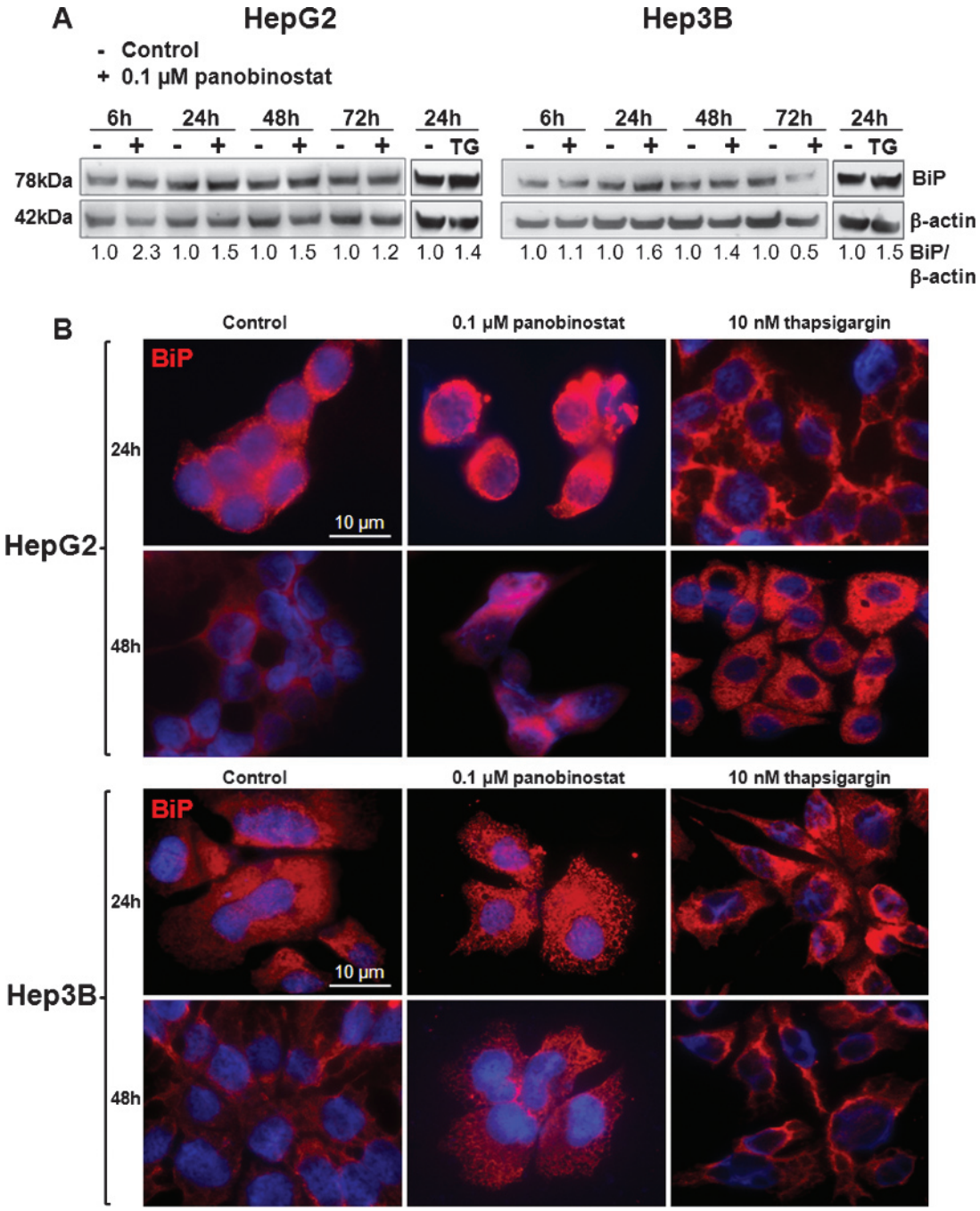

Figure 2. BiP protein level and localization analysis. (A) Western blot results of BiP in HepG2 (left) and Hep3B (right) cells, treated for 6, 24, 48, and 72 hours with 0.1 μM panobinostat and with 10 nM thapsigargin for 24 hours only. Densitometry results were normalized to β-actin content and are expressed relative to untreated controls set at 1.0. (B) Immunofluorescence analysis of BiP after 24 and 48 hours of treatment in HepG2 (upper panel) and Hep3B (lower panel) cells with 0.1 μM panobinostat and 10 nM thapsigargin, showing an increase and a different protein distribution in panobinostat-treated cells, comparable to 10 nM thapsigargin effect, used as a positive control. Immunofluorescence analysis has been performed under identical settings. Nuclei were stained with Hoechst 33342. Magnification is ×630, and scale bar represents 10 μm.

4°C, rinsed in Sörensen's buffer overnight, and post-fixed in 1% osmium tetroxide combined with 1.5% potassium ferricyanide [22] for 4 hours (4°C). Following dehydration in graded series of ethanol and propylene oxide, cell pellets were placed in capsules and polymerized at 60 and 80°C for 24 hours each. Single or serial silver ultrathin sections (approximately 70 nm) were cut, mounted on slot grids (oval hole; Plano, Wetzlar, Germany), and stained with lead citrate and uranyl acetate. Section thickness was determined using the interference color of sections floating on water [23] and the minimal folds method [24]. Ultrathin sections were examined with a Zeiss 906 electron microscope (LEO, Oberkochen, Germany) from 2156 to 35570 magnifications. Images created with electron microscopy were digitalized with Agfa SnapScan e50 scanner (Agfa-Gevaert, Mortsel, Belgium) and adapted for brightness and contrast by Adobe Photoshop 6.0 (Adobe

Table 1. Quantification of BiP Immunofluorescence Signals.

		Mean	SD	SEM	ANOVA
HepG2					
24 hours	Control	36.10	7.87	0.22	
	0.1 μM Panobinostat	54.62	0.80	0.01	0.03
	10 nM Thapsigargin	42.20	1.61	0.04	0.15
48 hours	Control	11.05	2.94	0.27	
	0.1 μM Panobinostat	50.35	6.90	0.14	0.00
	10 nM Thapsigargin	39.22	5.13	0.13	0.00
Hep3B					
24 hours	Control	26.67	2.88	0.11	
	0.1 μM Panobinostat	34.75	6.84	0.20	0.09
	10 nM Thapsigargin	42.12	3.67	0.09	0.00
48 hours	Control	8.70	3.73	0.43	
	0.1 μM Panobinostat	26.82	1.84	0.07	0.00
	10 nM Thapsigargin	38.02	4.96	0.13	0.00

The immunofluorescence cytosolic signal of BiP shows a significant increase in panobinostat- and thapsigargin-treated cell lines, especially after 48 hours ($P < .05$), whereas heterogeneous expression patterns are observed at the 24-hour time point.

Systems Incorporated, San Jose, CA) software. Black/white plates were created by using CorelDraw software (CorelDraw version 11; Corel Corporation, Ottawa, Ontario).

Statistical Analysis

Statistical analysis was performed using SPSS 15.0.1 for Windows (SPSS Inc, Chicago, IL). The *t* test and univariate analysis of variance (ANOVA, Bonferroni procedure) were used to test for differences between two and more groups of samples, respectively. $P < .01$ and $P < .05$ were regarded as significant.

Results

Panobinostat Induced mRNA Expression of ER Stress–Related Factors

We have previously demonstrated that HepG2 and Hep3B cells respond significantly to 0.1 μM panobinostat treatment, with a decrease of cell proliferation and activation of apoptosis that was not mediated by canonical pathways. Moreover, preliminary results suggested the involvement of alternative apoptotic pathways, like UPR and ER stress [10]. On the basis of our previous data, we investigated here the induction of these pathways in more detail.

First, we analyzed the expression levels of the ER stress–related factors IRE1α and IRE1β, two isoforms of IRE1, and of the molecular chaperone BiP in both cell lines, after treatment with 0.1 μM panobinostat from 6 to 72 hours (Figure 1, *A* and *B*).

The expression of IRE1α was induced already after 6 hours of treatment with panobinostat in both cell lines and it increased significantly after 48 hours in HepG2, while it was stable after 72 hours in Hep3B cells; BiP transcript slightly increased after 6 hours and its level was almost stable after 48 hours in both cell lines. IRE1β was not expressed

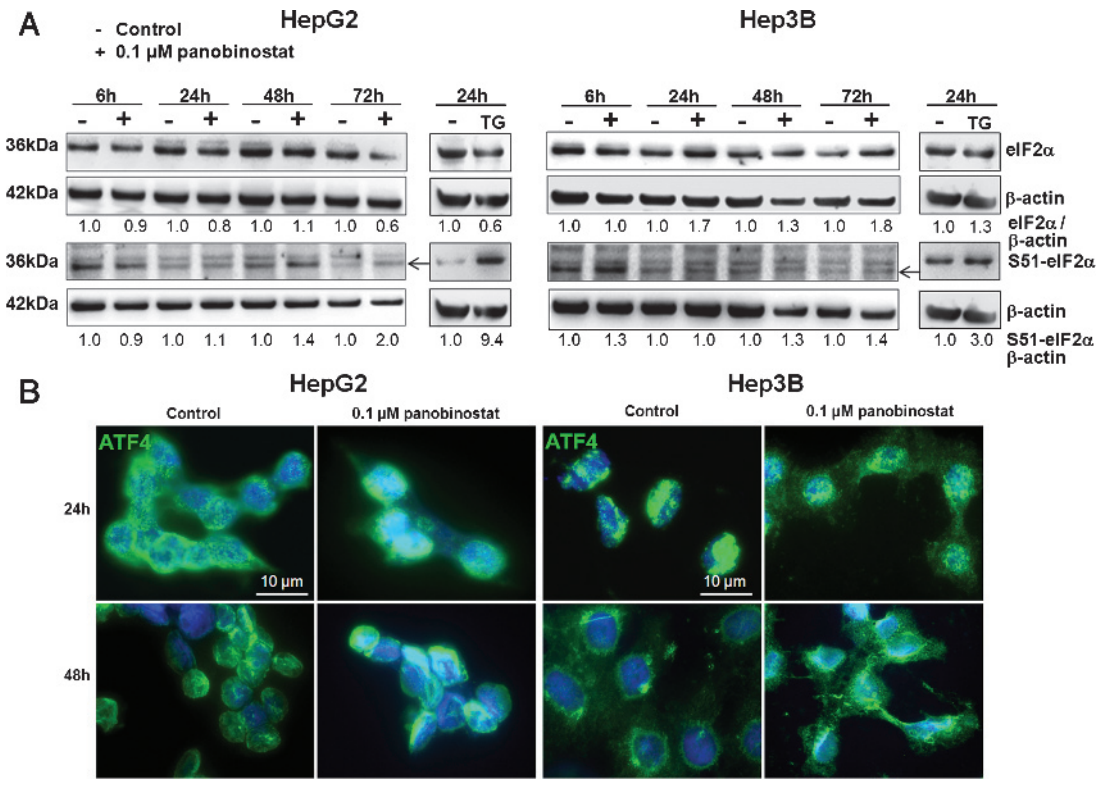

Figure 3. Evaluation of eIF2α protein activation and immunofluorescence analysis for ATF4. Western blot analysis reveals activation of eIF2α in both HCC cell lines after treatment with 0.1 μM panobinostat for 6, 24, 48, and 72 hours and with 10 nM thapsigargin for 24 hours. (A) Arrows indicate the specific band for S51-eIF2α. Densitometry results were normalized to β-actin content and are expressed relative to untreated controls set at 1.0. (B) HepG2 (left panel) and Hep3B (right panel) cells were treated for 24 and 48 hours with 0.1 μM panobinostat and the immunofluorescence results show an increase of ATF4 and its nuclear localization in both cell lines. Immunofluorescence analysis has been performed under identical settings. Nuclei were stained with Hoechst 33342. Magnification is ×630, and scale bar represents 10 μm.

Table 2. Quantification of Cytoplasmic and Nuclear ATF4 Immunofluorescence Signals.

		Cytosol				Nuclear			
		Mean	SD	SEM	*T* Test	Mean	SD	SEM	*T* Test
HepG2									
24 hours	Control	70.54	6.43	0.09		34.66	6.49	0.19	
	0.1 μM Panobinostat	66.58	8.33	0.12	0.19	114.82	25.65	0.22	0.00
48 hours	Control	101.54	10.05	0.10		12.82	3.03	0.24	
	0.1 μM Panobinostat	116.67	10.64	0.09	0.03	92.42	16.03	0.17	0.00
Hep3B									
24 hours	Control	120.75	6.20	0.05		46.85	8.92	0.19	
	0.1 μM Panobinostat	96.32	8.65	0.09	0.007	94.35	19.64	0.21	0.01
48 hours	Control	78.30	5.50	0.07		20.90	5.10	0.24	
	0.1 μM Panobinostat	79.67	9.96	0.12	0.444	69.73	8.80	0.13	0.00

Quantification of immunofluorescence signals shows a tendentious decrease of cytoplasmic signals between treated and untreated cell lines after 24 hours, whereas a significant increase of nuclear signals is found in the panobinostat-treated cell lines throughout all time periods ($P < .05$).

in both cell lines (data not shown). Furthermore, transcription factors ATF4, which promotes UPR gene expression [14,18], and CHOP, the best characterized proapoptotic factor related to the ER stress pathway [25], were analyzed. ATF4 level increased after 48 hours of treatment with panobinostat in both cell lines but did not reach statistical significance. In contrast, CHOP was significantly upregulated starting already after 24 hours of treatment in both cell lines but decreased to control level after 72 hours (Figure 1, *C* and *D*).

ER stress markers were confirmed to be strongly upregulated after 10 nM thapsigargin treatment, a sarcoplasmic/ER Ca^{2+}-dependent ATPase pump inhibitor, which was used as positive control of ER stress induction (Figure W1, *A* and *B*).

To confirm our previously published data [10], the effect of panobinostat in HepG2 and Hep3B cell lines was compared to thapsigargin treatment by using the impedance-based real-time cell viability analysis with the xCELLigence System (Figure W1, *C* and *D*). Obtained data revealed that panobinostat caused a reduction of normalized cell index comparable to the reduction caused by thapsigargin treatment, confirming that panobinostat induces cell death with an ER stress resembling mode of action.

Panobinostat Treatment Induced Chaperone Up-regulation and Attenuation of Protein Translation

We further analyzed the key players of UPR mechanism, to clarify the exact mechanisms induced by panobinostat treatment in HCC cell lines. BiP protein level was evaluated by Western blot (Figure 2*A*) and by immunofluorescence (Figure 2*B*) after treatment with 0.1 μM panobinostat and 10 nM thapsigargin. Its level increased already after 6 hours of treatment in HepG2 cells (2.3-fold increase, as quantified by densitometric analysis) followed by stabilization until 72 hours. In Hep3B, BiP increased after 24 and 48 hours of treatment (1.6- and 1.4-fold increase; Figure 2*A*). Thapsigargin treatment induced the increase of BiP protein level comparable to panobinostat effects in both cell lines (1.4- and 1.5-fold increase, respectively; Figure 2*A*).

The immunofluorescence micrographs, acquired at 24 and 48 hours of treatment, confirmed the significant increase of BiP in both cell lines, which was also calculated by immunofluorescence signal quantification (Table 1). Its increase after treatment with panobinostat was comparable to or moderately stronger than the increase visualized in cells incubated with 10 nM thapsigargin (Figure 2*B*). Moreover, panobinostat caused an alteration of BiP cellular distribution, inducing the formation of brighter aggregate structures in the cytosolic compartment of treated cells (Figure 2*B*).

ER stress induced in HCC cells by treatment with panobinostat was furthermore confirmed by Western blot analysis of eIF2α protein level, its Ser51-phosphorylated active form, and its target ATF4 (Figure 3, *A* and *B*). eIF2α densitometry analysis showed a stable level in HepG2 until 48 hours of treatment and a 1.7-fold increase in Hep3B after 24 hours of treatment. Interestingly, panobinostat induced an increase of Ser51-eIF2α after 48 hours in both cell lines (Figure 3*A*), indicating the involvement of active eIF2α after DACi treatment. Treatment with 10 nM thapsigargin induced solely a strong increase of the eIF2α active form Ser51-eIF2α in both cell lines (Figure 3*A*).

Immunofluorescence staining of ATF4 after treatment with panobinostat showed not only an increase of its expression in both cell lines, as confirmed by fluorescent signal quantification and by PCR, but also a strong and significant localization in the nuclear compartment (Figures 3*B* and W2 and Table 2), suggesting its translocation to the nuclei, where it can perform its activity. Additionally, ATF4 protein expression was evaluated by Western blot in cytosolic and nuclear fractions (Figure W3*A*) up to 72 hours of treatment with panobinostat, confirming the strong increase of this protein in the nuclear compartment in both cell lines. Surprisingly, ATF4 protein level slightly increased also in the cytosolic fraction; thapsigargin induced the increase of ATF4 in both cellular compartments and in both cell lines.

Panobinostat Activated IRE1α/XBP-1 Arm of UPR

During ER stress conditions, IRE1α, another essential UPR player, is activated through autophosphorylation after BiP dissociation.

We further investigated IRE1α protein level and its downstream target XBP-1. In Figure 4, we show that both IRE1α and its active Ser724-phosphorylated form significantly increased in HepG2 (A) and Hep3B (B) cells after 24 and 48 hours of panobinostat treatment and verified this by immunofluorescence signal quantification (Table 3), confirming the involvement of this factor in UPR activation mediated by panobinostat. Moreover, we observed that panobinostat treatment induced a reorganization of Ser724-phosphorylated IRE1α, which appeared with a spotted distribution (Figure 4, *A* and *B*; enlargement example depicted for Hep3B after a 24-hour treatment). IRE1α and its Ser724-phosphorylated form were further analyzed by Western blot after 72 hours of treatment with panobinostat, displaying an increase at 24 and 48 hours in HepG2 cells and

stable levels in Hep3B cells (Figure W3*B*); thapsigargin was used as a positive control.

IRE1α, once active, can catalyze the splicing of XBP-1 to generate an active transcription factor with higher transactivating activity [26,27]. Panobinostat treatment was able to induce XBP-1 splicing already after 6 hours of treatment in both cell lines (Figure 4*C*). The spliced form of XBP-1 (XBP-1s) strongly increased after 48 hours in HepG2, while the unspliced form (XBP-1u) was only reduced in

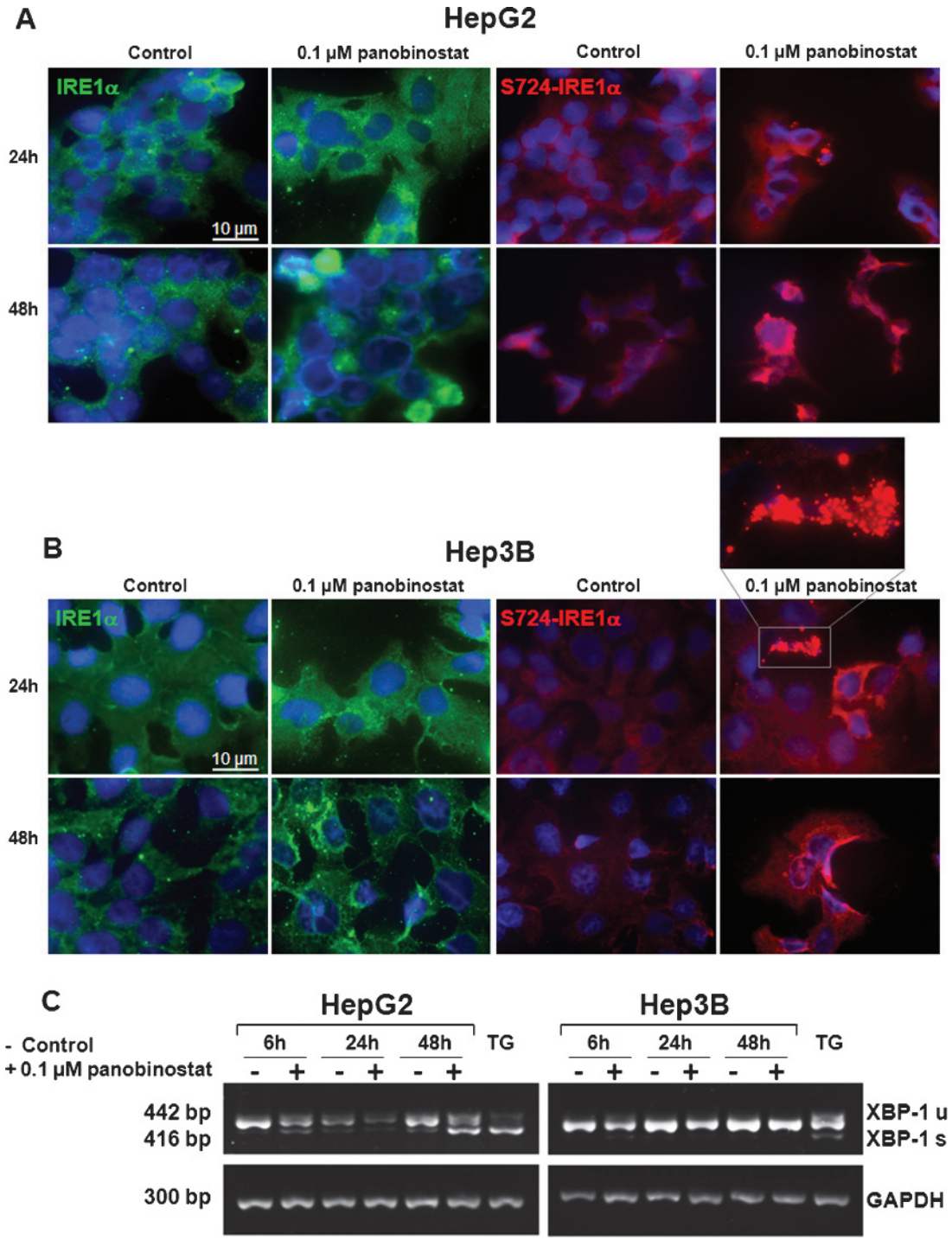

Figure 4. Analysis of IRE1α/XBP1 involvement. Immunofluorescence results of IRE1α and its phosphorylated form in HepG2 (A) and Hep3B (B) cell lines after 24 and 48 hours of treatment with 0.1 μM panobinostat. The results indicate that panobinostat induces an increase of both the total and the phosphorylated form of IRE1α and a spotted distribution of this protein (enlargement showed for phospho-IRE1α, B). Immunofluorescence analysis has been performed under identical settings. Nuclei were stained with Hoechst 33342. Magnification is ×630, and scale bar represents 10 μm. RT-PCR analysis of total RNA isolated from HepG2 and Hep3B cells treated with 0.1 μM panobinostat for 6, 24, and 48 hours (C). For this experiment, primers detecting both unspliced (XBP-1u, 442 bp) and spliced (XBP-1s, 416 bp) forms of XBP-1 mRNA were used. Both cell lines have been treated for 24 hours with 10 nM thapsigargin used as a positive control. Levels of GAPDH mRNA were used as a control for mRNA concentration.

Table 3. Quantification of IRE1α and Ser724-IRE1α Immunofluorescence Signals.

		IRE1α				S724-IRE1α			
		Mean	SD	SEM	*T* Test	Mean	SD	SEM	*T* Test
HepG2									
24 hours	Control	37.30	8.46	0.23		3.17	0.83	0.26	
	0.1 μM Panobinostat	61.40	10.56	0.17	0.02	19.02	5.27	0.28	0.00
48 hours	Control	26.32	9.16	0.35		4.53	2.27	0.50	
	0.1 μM Panobinostat	41.87	9.82	0.23	0.09	22.88	4.82	0.21	0.01
Hep3B									
24 hours	Control	13.22	7.98	0.60		1.75	1.47	0.84	
	0.1 μM Panobinostat	32.70	6.05	0.18	0.02	35.02	7.60	0.22	0.00
48 hours	Control	9.50	4.75	0.50		4.10	2.61	0.64	
	0.1 μM Panobinostat	16.20	4.35	0.27	0.06	10.53	1.30	0.12	0.01

After treatment with panobinostat, an increase of IRE1α signal is observed in HepG2 and Hep3B cell lines reaching a significant level only after 24 hours ($P < .05$). For the phosphorylated form Ser724-IRE1α, a significant increase of this protein is demonstrated during all time points investigated in both cell lines ($P < .05$).

Hep3B after 24 and 48 hours of treatment (Figure 4*C*). Panobinostat effect was merely comparable to 10 nM thapsigargin effect in HepG2 cells at 48 hours of treatment.

Role of CHOP in Panobinostat-Induced Effects

We, then, investigated a possible involvement of CHOP, a transcription factor triggering cell death in protracted ER stress *scenario*, in the mechanism induced by panobinostat treatment. Protein level of CHOP, analyzed by immunofluorescence, increased significantly after 24 and 48 hours of treatment in both cell lines (Figure 5*A* and W4 and Table 4). Moreover, panobinostat treatment was comparable to or even stronger than thapsigargin inducing a clear nuclear localization of CHOP (Figure 5*A* and Table 4).

Furthermore, CHOP protein level, evaluated by Western blot in cytosolic and nuclear fractions after 72 hours of treatment with panobinostat, proved the strong increase in the nuclear compartment and a stable level in the cytosolic fraction of HepG2 cells and its increase in both fractions of Hep3B cells. Surprisingly, thapsigargin induced CHOP increase only in the cytosolic fraction of both cell lines (Figure W3*A*).

Since panobinostat was able to strongly upregulate CHOP at both transcriptional (Figure 1, *C* and *D*) and translational (Figure 5*A*) levels, and since it has been shown that CHOP plays a fundamental role in mediating apoptosis, we evaluated the effects of CHOP knockdown on cell viability by using a specific CHOP siRNA (80% of knockdown efficiency; data not shown) alone and in combination with 0.1 μM panobinostat and analyzed cellular proliferation with the xCELLigence System. CHOP knockdown did not recover the cytotoxic effects of panobinostat in both cell lines (Figure 5*B*).

ER Stress–Related Cell Death

Sustained or massive ER stress can lead to cell death, and at least three pathways have been proposed to be involved in ER stress–mediated apoptosis: CHOP, tumor necrosis factor receptor–associated factor-2/apoptosis signaling kinase 1/JNK, and caspase-12 activation [25]. IRE1α activation can result in JNK phosphorylation, which is then activated and can exert its proapoptotic effects. Our previous work demonstrated that panobinostat treatment was able to induce a transient JNK phosphorylation in HepG2 and Hep3B cell lines [10]. To elucidate JNK involvement in panobinostat-induced cell death, we used the specific ATP-competitive JNK inhibitor SP600125 and we evaluated its effect on HCC cellular proliferation alone and in combination with panobinostat. SP600125 alone showed no cytotoxic effects in both cell lines (Figure 6, *A* and *B*) or reverted the effects of panobinostat partially, especially in HepG2 within the first 24 hours of treatment (Figure 6, *C* and *D*), indicating an early involvement of this mitogen-activated protein kinase in panobinostat treatment response due to the transient increase of its phosphorylated form [10].

To further elucidate how panobinostat was able to terminally induce cell death in HCC cells, we analyzed ER stress–related caspase-12 and caspase-4.

Panobinostat induced a significant activation of both caspases ($P < .01$) in Hep3B and a slight activation in HepG2 cells (Figure 7, *A* and *B*). The addition of specific caspase-12 and caspase-4 inhibitors neutralized caspase-12 activation in Hep3B and caspase-4 activation in both cell lines determined by panobinostat treatment (Figure 7, *A* and *B*). Moreover, the inhibition of caspase-12 reduced panobinostat effects on cell death in HepG2 cells (Figure 7*C*) and the inhibition of both caspase-12 and caspase-4 led to a slight recovery from panobinostat-induced cell death in Hep3B (Figure 7*D*). We have also investigated the activity of the initiator caspase-8 (Figure 7, *C* and *D*) and the effector caspase-3/7 (Figure 7, *E* and *F*). Interestingly, the inhibition of both caspase-12 and caspase-4 blocked significantly caspase-8 activation in both cell lines ($P < .01$ in both cell lines with caspase-12 inhibitor and in Hep3B with caspase-4 inhibitor; Figure 7, *C* and *D*).

In addition, induced caspase-3/7 activity after panobinostat treatment was strongly inhibited by caspase-4 inhibitor ($P < .01$ in both cell lines with caspase-12 and caspase-4 inhibitors; Figure 7, *E* and *F*). The results referring to caspase-3/7 activity in Hep3B cells after addition of 0.1 μM panobinostat and caspase-12 inhibitor have been already published in our previous work [10].

Panobinostat Induced Altered ER Morphology

The induction of ER stress was also supported by qualitative ultrastructure analysis using transmission electron microscopy (TEM). Micrographs of untreated HepG2 and Hep3B cells showed regular arrangement of ER cisternae distributed randomly throughout the cytoplasm (Figure 8, *A* and *B*, *left panel*). After 24 and 48 hours of treatment with 0.1 μM panobinostat, ER cisternae appeared fragmented and extremely disorganized in both cell lines. Note the enlargements in Figure 8 (*A* and *B*, *right panels*); the arrows indicate ER cisternae.

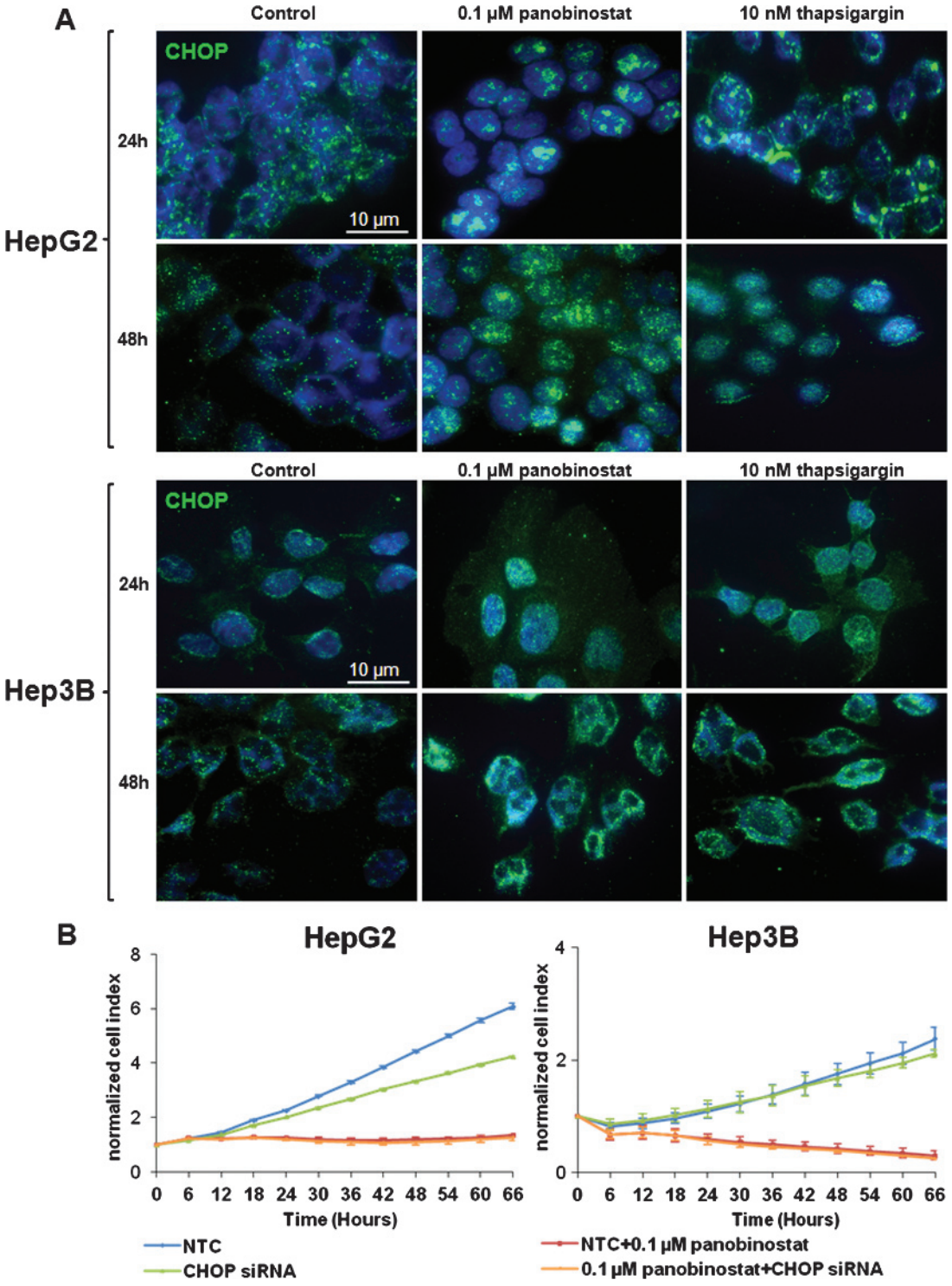

Figure 5. (A) Role of CHOP in panobinostat-induced cell death. Immunofluorescence analysis of CHOP after 24 and 48 hours of treatment in HepG2 (upper panel) and Hep3B (lower panel) cells with 0.1 μM panobinostat, showing an increase and the nuclear localization of CHOP in panobinostat-treated cells, comparable to 10 nM thapsigargin effect used as a positive control. Immunofluorescence analysis has been performed under identical settings. Nuclei were stained with Hoechst 33342. Magnification is $\times$630, and scale bar represents 10 μm. For the impedance-based real-time cell viability study (B), HepG2 and Hep3B cells were cultured in E-plates and simultaneously transfected with a specific CHOP siRNA; panobinostat at 0.1 μM was added after approximately 24 hours. Cell index was normalized to the time point of treatment with panobinostat. Cell index was determined continuously for additional 70 hours. AllStars Negative Control was included as nonsilencing control. Results are means $\pm$ SD from triplicates.

Table 4. Quantification of Nuclear CHOP Immunofluorescence Signals.

		Mean	SD	SEM	ANOVA
HepG2					
24 hours	Control	14.70	4.55	0.31	
	0.1 μM Panobinostat	99.86	28.07	0.28	0.00
	10 nM Thapsigargin	118.72	13.00	0.11	0.00
48 hours	Control	5.10	2.64	0.52	
	0.1 μM Panobinostat	96.52	11.89	0.12	0.00
	10 nM Thapsigargin	87.50	6.60	0.07	0.00
Hep3B					
24 hours	Control	30.65	5.65	0.18	
	0.1 μM Panobinostat	76.27	11.91	0.16	0.01
	10 nM Thapsigargin	55.73	5.77	0.10	0.01
48 hours	Control	23.02	5.50	0.24	
	0.1 μM Panobinostat	114.70	10.84	0.09	0.00
	10 nM Thapsigargin	93.75	12.74	0.14	0.00

The nuclear expression of CHOP is significantly higher in panobinostat- and thapsigargin-treated cell lines ($P < .05$) compared to controls. Interestingly, the immunofluorescence signal of CHOP in the nuclei of panobinostat-treated Hep3B cells is significantly higher compared to thapsigargin treatment used as positive control ($P < .05$).

Discussion

HCC is the fifth most common tumor and the third leading cause of cancer-related deaths worldwide [28]. HCC is still associated with poor prognosis and only around 30% of diagnosed patients are considered eligible for potential curative treatment. The tyrosine kinase inhibitor sorafenib was the first systemic targeted therapy approved by the US Food and Drug Administration for the treatment of advanced HCC despite its limitations, like low overall response rates and high toxicity [29].

Sustained efforts have been put into discovering new targets and molecular pathways to develop novel drugs. Since epigenetic modifications, such as hyperacetylation of histones and nonhistone proteins, in addition to classic genetic mechanisms, have been discovered to be involved in tumor development and progression, DACis have been considered as novel attractive therapeutic approaches for several malignancies [30], including also HCC. DACis are a heterogeneous class of drugs able to regulate the acetylation status of diverse intracellular proteins, like histones, transcription factors, and molecular chaperones [31,32]. The hydroxamic acid

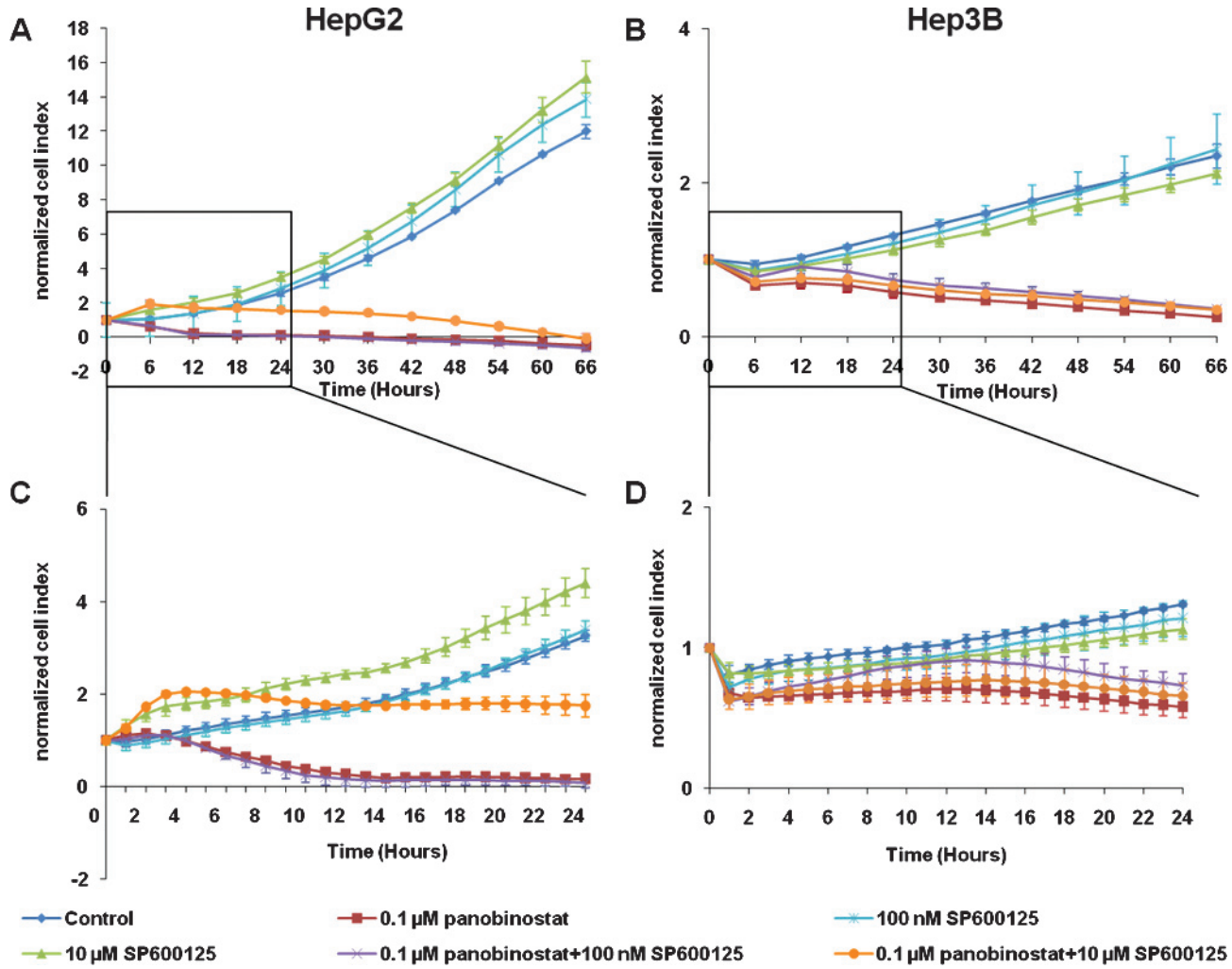

Figure 6. Involvement of JNK in panobinostat-induced cell death. HepG2 (A and C) and Hep3B (B and D) cells were cultured in E-plates and, after approximately 24 hours, treated with 0.1 μM panobinostat and 100 nM and 10 μM SP600125. Cell index was normalized to the time point of treatment. Cell index was determined continuously for additional 70 hours. In C and D, the effects of the compounds during the first 24 hours of treatment are depicted, displaying that SP600125 is able to partially recover the early effects of panobinostat in both cell lines.

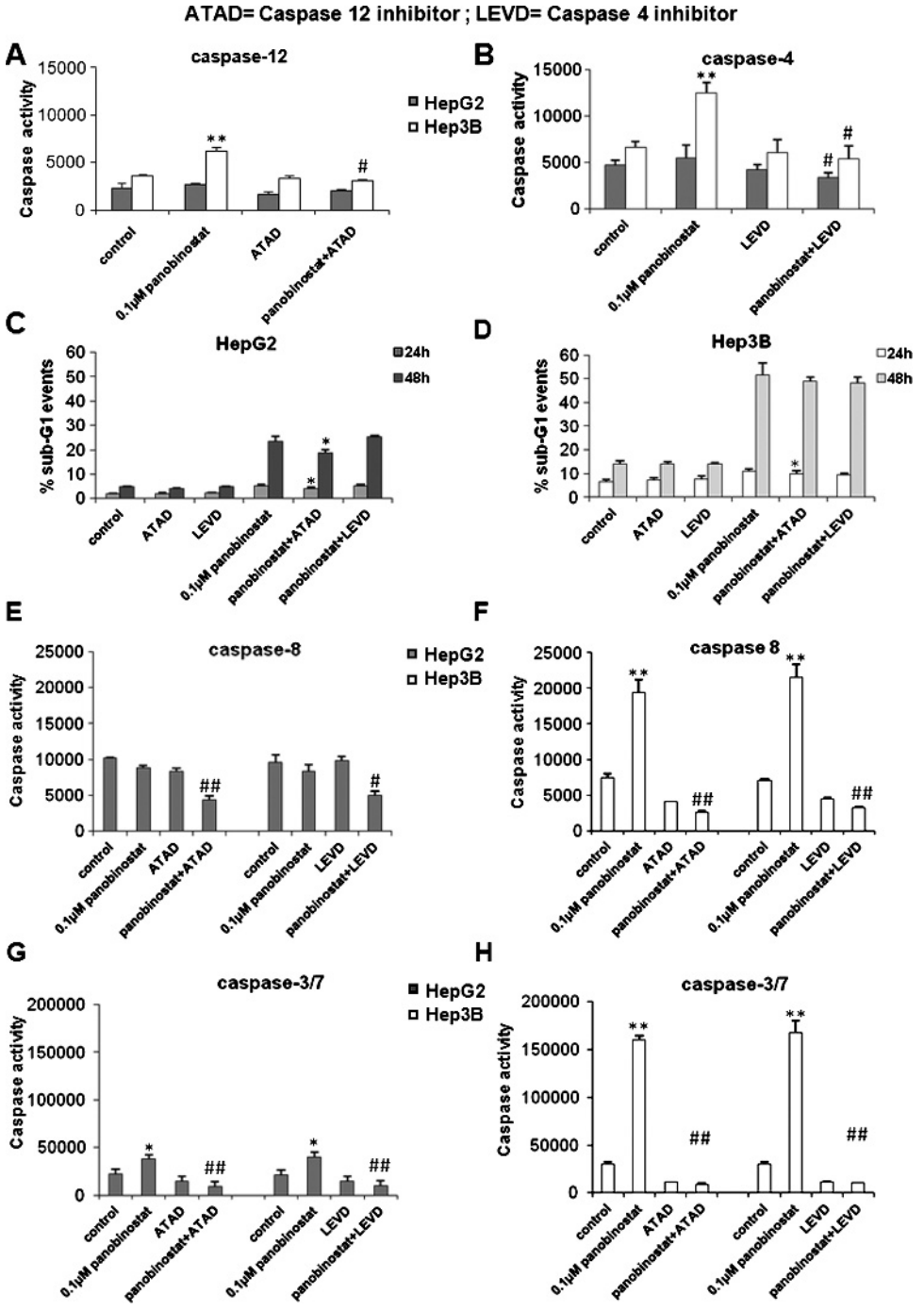

Figure 7. Panobinostat induces ER stress–mediated caspase activation. Caspase-12 (A) and caspase-4 (B) activities were analyzed using specific fluorimetric assays after treatment of HepG2 and Hep3B cells with 0.1 μM panobinostat and caspase-12 (Z-ATAD-FMK) and caspase-4 (Z-LEVD-FMK) inhibitors for 48 hours. The percentage of apoptotic cells was determined by measuring the fraction of nuclei with a subdiploid DNA content after treatment with 0.1 μM panobinostat and caspase-12 (Z-ATAD-FMK) and caspase-4 (Z-LEVD-FMK) inhibitors for 48 hours (C and D). Caspase-8 activity was analyzed in HepG2 (E) and Hep3B (F) cells using a luminescent assay. Downstream activity of caspase-3/7, analyzed in HepG2 (G) and Hep3B (H) cells through a luminescent assay, decreases after inhibition of caspase-12 with Z-ATAD-FMK and of caspase-4 with Z-LEVD-FMK. $^{*}P < .05$ *versus* control or $^{\#}P < .05$ *versus* panobinostat alone; $^{**}P < .01$ *versus* control or $^{\#\#}P < .01$ *versus* panobinostat alone.

panobinostat (LBH589) is among the most potent DACis, with nanomolar DAC inhibitory activity and a strong antitumor ability demonstrated for hematologic and solid malignancies *in vitro*, *in vivo*, and in clinical trials [2,33]. Despite the recent intensive studies on DACi, the exact mechanisms of action of these compounds are not completely understood.

It has been shown that through the inhibition of deacetylase activity, they can affect a broad range of cellular pathways, modulating cell cycle arrest, cell differentiation, canonical apoptotic pathways, and alternative cell death mechanisms [33–35]. Furthermore, DACis like vorinostat and panobinostat are able, solely or in combination with other drugs, to contribute to UPR and to induce ER stress–mediated

apoptosis, for instance through the acetylation of heat shock proteins like BiP [6,7,10,36,37].

Different physiological and pathologic conditions can compromise ER functions, leading to the activation of a specific and complex signaling pathway, named UPR, with following transcriptional up-regulation of genes encoding molecular chaperones, oxidoreductases, and ER-associated degradation components [38], in attempt to re-establish ER homeostasis.

UPR is orchestrated by three distinct stress sensors located at the ER membrane, IRE1α, PERK, and ATF6α [14], that are kept inactive by the chaperone BiP under physiologic conditions [10,15]. As a consequence of stress, they dissociate from BiP and transduce the UPR signal, while the chaperone binds the hydrophobic residues of unfolded proteins, to facilitate proper protein folding, to prevent protein aggregate formation, and to drive misfolded proteins to the final proteasomal degradation [39]. However, if stress is protracted and ER function is severely impaired, the organelle triggers apoptotic cell death. We have previously shown that panobinostat treatment was able to induce apoptotic cell death *in vitro* and *in vivo*, surprisingly, without the involvement of canonical pathways [4,10]. Here, we clearly demonstrate that panobinostat is able to induce alternative apoptotic cell death in two different HCC cell lines (HepG2 and Hep3B) through the activation of ER stress pathway. Its modality of action was comparable to thapsigargin, a sarcoplasmic/ER Ca^{2+}-dependent ATPase pump inhibitor, used as an ER stress inducer [40]. In both HCC cell lines, panobinostat treatment induces the early up-regulation of BiP transcript and the protracted increase of its protein level, probably due to posttranslational modifications, e.g., acetylation, which enhances its protein stability [7,36]. In our model, panobinostat upregulates and induces IRE1α, a transmembrane protein harboring a dual enzymatic activity of protein kinase and endoribonuclease [41]. The endoribonuclease activity is involved in the processing of XBP-1 mRNA and the Ser/Thr kinase domain is implicated in the recruitment of tumor necrosis factor receptor–associated factor-2/apoptosis signaling kinase 1 to mediate the activation of JNK and of nuclear factor κB [42]. IRE1α, once free from BiP binding, can be activated through trans-autophosphorylation on Ser724 [41] and further catalyzes XBP-1 splicing, which is clearly

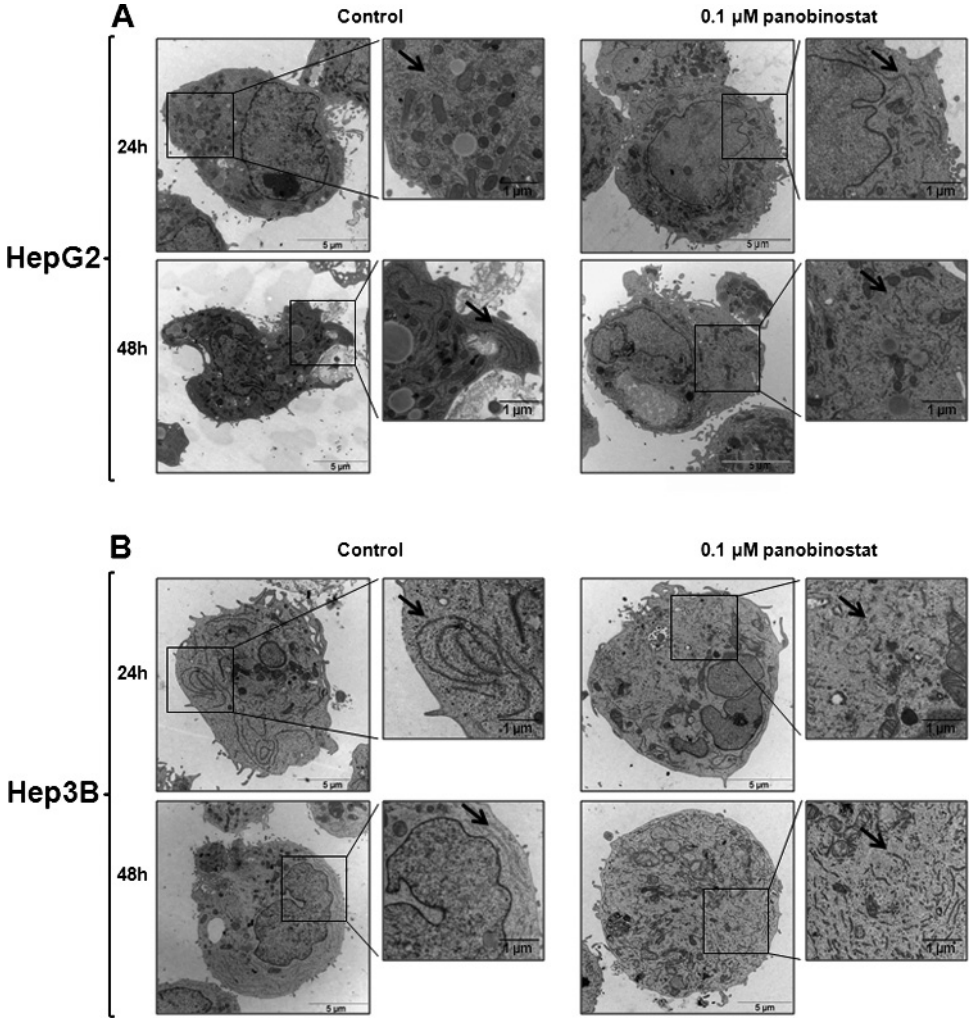

Figure 8. TEM analysis of ER morphology. HepG2 (A) and Hep3B (B) cells were treated for 24 and 48 hours with 0.1 μM panobinostat and then processed as described in Materials and Methods section. ER distribution and morphology appear extremely disorganized with fragmented cisternae in both HCC cells after treatment with panobinostat. This pattern is highlighted by an enlargement of each picture (inserts). The black arrows indicate the areas of particular interest. Magnification is ×2156 and ×35570, and scale bars represent 5 μm and 1 μm, respectively.

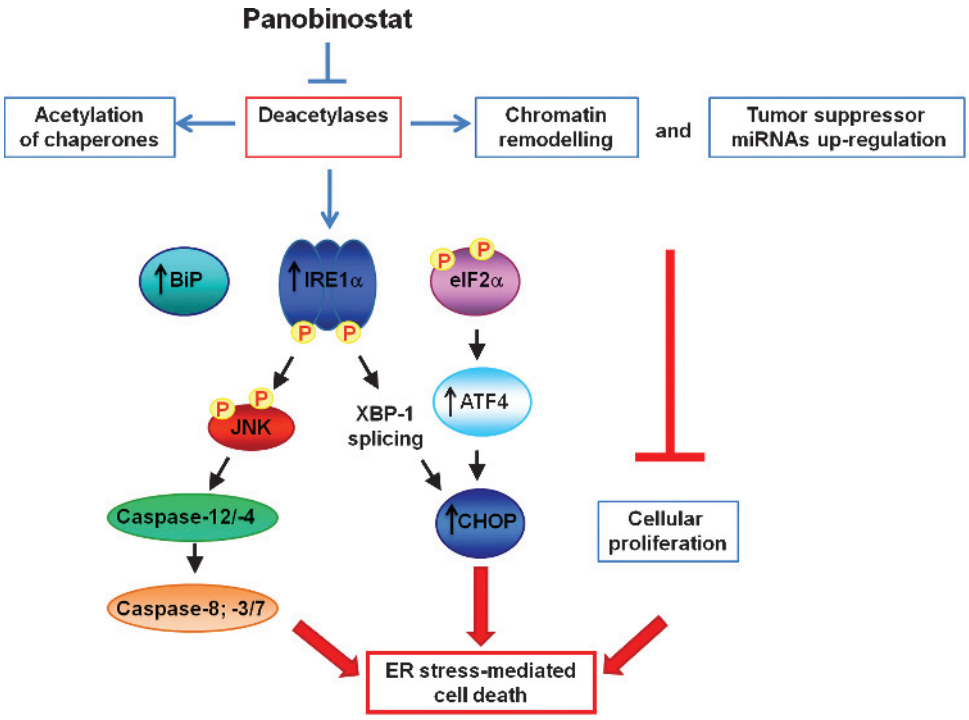

Figure 9. Schematic representation of panobinostat effects in liver cancer models. Panobinostat is able to inhibit DACs, inducing acetylation of histones and non-histone proteins, leading to chromatin remodeling and tumor suppressor miRNA up-regulation, both contributing to block cell proliferation and to induce alternative cell death. In particular, the acetylation of molecular chaperones, like BiP, together with modulation of ER stress marker expression, triggers an ER stress–mediated cell death, through the involvement of IRE1α/XBP-1/JNK, eIF2α/ATF4, CHOP, and caspase-12/4, caspase-8, and caspase-3/7.

detectable in HepG2 after panobinostat treatment. Then, XBP-1s can induce the expression of several genes involved in different aspects of UPR [18,26,43], regulating not only the adaptive response to ER stress but also apoptotic cell death. In LLC-PK1 cells, induction of CHOP, activation of XBP-1, and phosphorylation of JNK were identified as possible downstream events responsible for apoptosis [44]. Moreover, XBP-1 is known to activate the transcription of CHOP [25]. In Hep3B cells, which differ from HepG2 in being p53 deficient, XBP-1s is detectable only after 6 hours of panobinostat treatment, but so far there is no evident correlation between p53 expression and XBP-1 splicing. Further analyses are needed to clarify this aspect.

Moreover, at high stress signaling levels, IRE1α may contribute to membrane-associated mRNA degradation through a process named regulated IRE1α-dependent decay that could first defend cells against ER stress by limiting new protein translation and further promote apoptotic mechanism in the setting of severe ER stress [18].

During UPR, an ER resident protein kinase (PERK), phosphorylates the α subunit of eIF2α, which alleviates ER stress through attenuation of global mRNA translation, by decreasing the overload of misfolded proteins and favoring the expression of ATF4 transcription factor [14,18]. Panobinostat treatment leads to eIF2α phosphorylation in both HCC cell lines and to ATF4 up-regulation and nuclear translocation, where it can regulate the expression of target genes, like *CHOP* [15].

Additionally, the transcription factor CHOP, one of the pro-apoptotic members of the ER stress–mediated apoptotic pathway [25,45], strongly increases after panobinostat treatment in HCC cells. CHOP promotes the transcription of some BH3-only and *growth arrest and DNA damage–inducible 34* genes and represses the expression of the antiapoptotic *Bcl-2* gene, thus contributing to the induction of canonical apoptosis [46]. Surprisingly, despite the ability of panobinostat to upregulate CHOP in HepG2 and Hep3B cells, this transcription factor is not the key player of panobinostat-induced cell death in our model, since its specific knockdown is not able to counteract panobinostat effects. This finding is in line with our previous results showing that panobinostat affected neither the mitochondrial potential nor Bcl-2 members' expression [10].

In addition to CHOP, JNK and caspase activation have also been implicated in ER stress–mediated apoptosis [15,47]. In particular, it has been demonstrated that JNK mediates ER stress–related cell death through the activation of caspase-12, a murine member of the inflammatory group of caspase family localized in the ER [25,48–50]. Our results using the specific JNK inhibitor SP600125 show that this kinase is strongly implicated in the early response to panobinostat treatment, confirming our previously published results about its transient phosphorylation [10].

Our data suggest that the up-regulation of CHOP, together with the activation of JNK, contributes to panobinostat-induced cell death in HCC cell lines through the activation of the ER resident caspase-12. However, the role of caspase-12 in human is still under debate, since *human caspase-12* gene has a single-nucleotide polymorphism, which leads either to a truncated protein or to a full-length protein with no enzymatic activity [50,51]. Moreover, caspase-4, belonging to the same caspase-12 subfamily, was found in human to be localized to the ER membrane and activated specifically by ER stress inducers, showing a caspase-12 identical mechanism of action [49]. Here, we show that panobinostat is able to induce

caspase-12 and even stronger caspase-4 activation, which in turn triggers caspase-8 and caspase-3/7, leading to alternative apoptotic cell death.

Finally, panobinostat treatment induces clear ER morphology alterations in HepG2 and Hep3B cell lines, confirming ER stress induction. Indeed, during ER stress, the accumulation of unfolded proteins and the impairment of ER function can be clearly detected through morphologically fragmented and disorganized ER cisternae observed by TEM micrographs [52–54].

In summary, we present for the first time that the pan-DACi panobinostat causes an ER stress–mediated alternative cell death pathway in HCC cell lines HepG2 (TP53wt) and Hep3B (TP53null), through the involvement of BiP, IRE1α/XBP-1, and eIF2α/ATF4 axis, which triggers JNK and CHOP induction that finally activates caspase-12/4, caspase-8, and caspase-3/7, in a p53-independent manner (Figure 9). A role in the regulation of ER stress markers of other p53 family members, i.e., p63 or p73, has been recently shown [55,56] and cannot be excluded in our setting for panobinostat-induced effects.

Nevertheless, apoptotic cell death mechanisms under conditions of irreversible ER damage are only partially understood and may involve a series of additional complementary pathways [46].

It has been widely demonstrated that autophagy, an evolutionary conserved intracellular degradation pathway that plays a crucial role in eliminating long-lived proteins, recycling of cytoplasmic components, and removal of damaged organelles, is upregulated in response to ER stress [57,58]. In particular, the UPR can trigger and regulate autophagy at different stages to remove damaged ER [59,60]. Autophagy up-regulation during ER stress is activated to relieve the stress and to restore homeostasis of the ER. However, prolonged or unresolved ER stress results in activation of the apoptotic program [59]. Recent studies provided that panobinostat induces autophagy in a colon cancer model through the involvement of death-associated protein kinase 1, a positive regulator of autophagy activated in response to ER stress [59,61].

Moreover, various studies revealed that miRNAs, like miR-346 [62], miR-708 [63], or miR199a/214 [64], are possible regulators of cell death during ER stress [17] and that panobinostat, as well as other HDACis, could trigger the expression of miRNAs related to ER stress in different models [20,65–67].

Furthermore, panobinostat is able to affect a broad and diverse spectrum of signaling pathways, like cell cycle progression and cellular proliferation, for instance, through transcriptional regulation of p21/WAF1 (CDKN1A) [10] and promotion of tumor suppressor miRNA hsa-let-7b maturation, leading to the inhibition of the oncogene HMGA2 [20]. The high complexity of panobinostat effects culminate in cellular proliferation rate decrease and cell death promotion, presenting DACi as a new class of compounds that may significantly contribute to overcome the high resistance to treatment with conventional chemotherapeutic agents. Undoubtedly, additional analyses are required to elucidate their mechanism of action.

Acknowledgments

We are indebted to Susanne Lingelbach for her outstanding technical support and to Ansgar Schmidt from the Institute for Pathology, Philipps University of Marburg (Marburg, Germany), for his technical assistance at the fluorescence microscopy.

References

[1] Schattenberg JM, Schuchmann M, and Galle PR (2011). Cell death and hepatocarcinogenesis: dysregulation of apoptosis signaling pathways. *J Gastroenterol Hepatol* **26**(suppl 1), 213–219.

[2] Tan J, Cang S, Ma Y, Petrillo RL, and Liu D (2010). Novel histone deacetylase inhibitors in clinical trials as anti-cancer agents. *J Hematol Oncol* **3**, 5.

[3] Atadja P (2009). Development of the pan-DAC inhibitor panobinostat (LBH589): successes and challenges. *Cancer Lett* **280**, 233–241.

[4] Di Fazio P, Ocker M, and Montalbano R (2011). New drugs, old fashioned ways: ER stress induced cell death. *Curr Pharm Biotechnol* **13**, 2228–2234.

[5] Rao R, Nalluri S, Kolhe R, Yang Y, Fiskus W, Chen J, Ha K, Buckley KM, Balusu R, Coothankandaswamy V, et al. (2010). Treatment with panobinostat induces glucose-regulated protein 78 acetylation and endoplasmic reticulum stress in breast cancer cells. *Mol Cancer Ther* **9**, 942–952.

[6] Suzuki M, Endo M, Shinohara F, Echigo S, and Rikiishi H (2009). Enhancement of cisplatin cytotoxicity by SAHA involves endoplasmic reticulum stress-mediated apoptosis in oral squamous cell carcinoma cells. *Cancer Chemother Pharmacol* **64**, 1115–1122.

[7] Kahali S, Sarcar B, Fang B, Williams ES, Koomen JM, Tofilon PJ, and Chinnaiyan P (2010). Activation of the unfolded protein response contributes toward the antitumor activity of vorinostat. *Neoplasia* **12**, 80–86.

[8] Gahr S, Wissniowski T, Zopf S, Strobel D, Pustowka A, and Ocker M (2012). Combination of the deacetylase inhibitor panobinostat and the multi-kinase inhibitor sorafenib for the treatment of metastatic hepatocellular carcinoma—review of the underlying molecular mechanisms and first case report. *J Cancer* **3**, 158–165.

[9] Stewart AK (2012). Novel therapeutics in multiple myeloma. *Hematology* **17**(suppl 1), 105–108.

[10] Di Fazio P, Schneider-Stock R, Neureiter D, Okamoto K, Wissniowski T, Gahr S, Quint K, Meissnitzer M, Alinger B, Montalbano R, et al. (2010). The pan-deacetylase inhibitor panobinostat inhibits growth of hepatocellular carcinoma models by alternative pathways of apoptosis. *Cell Oncol* **32**, 285–300.

[11] Walter P and Ron D (2011). The unfolded protein response: from stress pathway to homeostatic regulation. *Science* **334**, 1081–1086.

[12] Wang HC, Huang W, Lai MD, and Su IJ (2006). Hepatitis B virus pre-S mutants, endoplasmic reticulum stress and hepatocarcinogenesis. *Cancer Sci* **97**, 683–688.

[13] Ron D and Walter P (2007). Signal integration in the endoplasmic reticulum unfolded protein response. *Nat Rev Mol Cell Biol* **8**, 519–529.

[14] Hetz C and Glimcher LH (2009). Fine-tuning of the unfolded protein response: assembling the IRE1α interactome. *Mol Cell* **35**, 551–561.

[15] Malhi H and Kaufman RJ (2011). Endoplasmic reticulum stress in liver disease. *J Hepatol* **54**, 795–809.

[16] Rutkowski DT and Kaufman RJ (2004). A trip to the ER: coping with stress. *Trends Cell Biol* **14**, 20–28.

[17] Gorman AM, Healy SJ, Jager R, and Samali A (2012). Stress management at the ER: regulators of ER stress-induced apoptosis. *Pharmacol Ther* **134**, 306–316.

[18] Tabas I and Ron D (2011). Integrating the mechanisms of apoptosis induced by endoplasmic reticulum stress. *Nat Cell Biol* **13**, 184–190.

[19] Engin F and Hotamisligil GS (2010). Restoring endoplasmic reticulum function by chemical chaperones: an emerging therapeutic approach for metabolic diseases. *Diabetes Obes Metab* **12**(suppl 2), 108–115.

[20] Di Fazio P, Montalbano R, Neureiter D, Alinger B, Schmidt A, Merkel AL, Quint K, and Ocker M (2012). Downregulation of HMGA2 by the pan-deacetylase inhibitor panobinostat is dependent on hsa-let-7b expression in liver cancer cell lines. *Exp Cell Res* **318**, 1832–1843.

[21] Kirkeby S and Thomsen CE (2005). Quantitative immunohistochemistry of fluorescence labelled probes using low-cost software. *J Immunol Methods* **301**, 102–113.

[22] Karnovsky M (1971). Use of ferrocyanide reduced osmium in electron microscopy. *Proc 14th Annu Meet Am Soc Cell Biol* 146a.

[23] Small J (1968). Measurement of section thickness. *Abstr 4th Eur Reg Conf Electron Microsc* **1**, 609–610.

[24] Peachey LD (1958). Thin sections. I. A study of section thickness and physical distortion produced during microtomy. *J Biophys Biochem Cytol* **4**, 233–242.

[25] Oyadomari S and Mori M (2004). Roles of CHOP/GADD153 in endoplasmic reticulum stress. *Cell Death Differ* **11**, 381–389.

[26] Yoshida H (2007). Unconventional splicing of XBP-1 mRNA in the unfolded protein response. *Antioxid Redox Signal* **9**, 2323–2333.

[27] Meister S, Schubert U, Neubert K, Herrmann K, Burger R, Gramatzki M, Hahn S, Schreiber S, Wilhelm S, Herrmann M, et al. (2007). Extensive immunoglobulin production sensitizes myeloma cells for proteasome inhibition. *Cancer Res* **67**, 1783–1792.

[28] Cao H, Phan H, and Yang LX (2012). Improved chemotherapy for hepatocellular carcinoma. *Anticancer Res* **32**, 1379–1386.
[29] Frenette C and Gish R (2012). Targeted systemic therapies for hepatocellular carcinoma: clinical perspectives, challenges and implications. *World J Gastroenterol* **18**, 498–506.
[30] Coradini D and Speranza A (2005). Histone deacetylase inhibitors for treatment of hepatocellular carcinoma. *Acta Pharmacol Sin* **26**, 1025–1033.
[31] Khan O and La Thangue NB (2012). HDAC inhibitors in cancer biology: emerging mechanisms and clinical applications. *Immunol Cell Biol* **90**, 85–94.
[32] Miller CP, Singh MM, Rivera-Del Valle N, Manton CA, and Chandra J (2011). Therapeutic strategies to enhance the anticancer efficacy of histone deacetylase inhibitors. *J Biomed Biotechnol* **2011**, 514261.
[33] Prince HM, Bishton MJ, and Johnstone RW (2009). Panobinostat (LBH589): a potent pan-deacetylase inhibitor with promising activity against hematologic and solid tumors. *Future Oncol* **5**, 601–612.
[34] Ocker M and Schneider-Stock R (2007). Histone deacetylase inhibitors: signalling towards p21cip1/waf1. *Int J Biochem Cell Biol* **39**, 1367–1374.
[35] Ocker M (2010). Deacetylase inhibitors—focus on non-histone targets and effects. *World J Biol Chem* **1**, 55–61.
[36] Rao R, Balusu R, Fiskus W, Mudunuru U, Venkannagari S, Chauhan L, Smith JE, Hembruff SL, Ha K, Atadja P, et al. (2012). Combination of pan-histone deacetylase inhibitor and autophagy inhibitor exerts superior efficacy against triple-negative human breast cancer cells. *Mol Cancer Ther* **11**, 973–983.
[37] Liu YL, Yang PM, Shun CT, Wu MS, Weng JR, and Chen CC (2010). Autophagy potentiates the anti-cancer effects of the histone deacetylase inhibitors in hepatocellular carcinoma. *Autophagy* **6**, 1057–1065.
[38] Ni M and Lee AS (2007). ER chaperones in mammalian development and human diseases. *FEBS Lett* **581**, 3641–3651.
[39] Lee AS (2007). GRP78 induction in cancer: therapeutic and prognostic implications. *Cancer Res* **67**, 3496–3499.
[40] Kamiya T, Obara A, Hara H, Inagaki N, and Adachi T (2011). ER stress inducer, thapsigargin, decreases extracellular-superoxide dismutase through MEK/ERK signalling cascades in COS7 cells. *Free Radic Res* **45**, 692–698.
[41] Lee AH and Glimcher LH (2009). Intersection of the unfolded protein response and hepatic lipid metabolism. *Cell Mol Life Sci* **66**, 2835–2850.
[42] Parmar VM and Schroder M (2012). Sensing endoplasmic reticulum stress. *Adv Exp Med Biol* **738**, 153–168.
[43] Acosta-Alvear D, Zhou Y, Blais A, Tsikitis M, Lents NH, Arias C, Lennon CJ, Kluger Y, and Dynlacht BD (2007). XBP1 controls diverse cell type- and condition-specific transcriptional regulatory networks. *Mol Cell* **27**, 53–66.
[44] Yokouchi M, Hiramatsu N, Hayakawa K, Kasai A, Takano Y, Yao J, and Kitamura M (2007). Atypical, bidirectional regulation of cadmium-induced apoptosis via distinct signaling of unfolded protein response. *Cell Death Differ* **14**, 1467–1474.
[45] Chakrabarti A, Chen AW, and Varner JD (2011). A review of the mammalian unfolded protein response. *Biotechnol Bioeng* **108**, 2777–2793.
[46] Hetz C (2012). The unfolded protein response: controlling cell fate decisions under ER stress and beyond. *Nat Rev Mol Cell Biol* **13**, 89–102.
[47] Nagai H, Noguchi T, Takeda K, and Ichijo H (2007). Pathophysiological roles of ASK1-MAP kinase signaling pathways. *J Biochem Mol Biol* **40**, 1–6.
[48] Szegezdi E, Fitzgerald U, and Samali A (2003). Caspase-12 and ER-stress-mediated apoptosis: the story so far. *Ann N Y Acad Sci* **1010**, 186–194.
[49] Jing G, Wang JJ, and Zhang SX (2012). ER stress and apoptosis: a new mechanism for retinal cell death. *Exp Diabetes Res* **2012**, 589589.
[50] Momoi T (2004). Caspases involved in ER stress-mediated cell death. *J Chem Neuroanat* **28**, 101–105.
[51] Lamkanfi M, Festjens N, Declercq W, Vanden Berghe T, and Vandenabeele P (2007). Caspases in cell survival, proliferation and differentiation. *Cell Death Differ* **14**, 44–55.
[52] Asselah T, Bieche I, Mansouri A, Laurendeau I, Cazals-Hatem D, Feldmann G, Bedossa P, Paradis V, Martinot-Peignoux M, Lebrec D, et al. (2010). *In vivo* hepatic endoplasmic reticulum stress in patients with chronic hepatitis C. *J Pathol* **221**, 264–274.
[53] Yang G, Sun Q, Teng Y, Li F, Weng T, and Yang X (2008). PTEN deficiency causes dyschondroplasia in mice by enhanced hypoxia-inducible factor 1α signaling and endoplasmic reticulum stress. *Development* **135**, 3587–3597.
[54] Vijayalakshmi K, Alladi PA, Ghosh S, Prasanna VK, Sagar BC, Nalini A, Sathyaprabha TN, and Raju TR (2011). Evidence of endoplasmic reticular stress in the spinal motor neurons exposed to CSF from sporadic amyotrophic lateral sclerosis patients. *Neurobiol Dis* **41**, 695–705.
[55] Zocchi L, Bourdon JC, Codispoti A, Knight R, Lane DP, Melino G, and Terrinoni A (2008). Scotin: a new p63 target gene expressed during epidermal differentiation. *Biochem Biophys Res Commun* **367**, 271–276.
[56] Pyati UJ, Gjini E, Carbonneau S, Lee JS, Guo F, Jette CA, Kelsell DP, and Look AT (2011). p63 mediates an apoptotic response to pharmacological and disease-related ER stress in the developing epidermis. *Dev Cell* **21**, 492–505.
[57] Jia W, Pua HH, Li QJ, and He YW (2011). Autophagy regulates endoplasmic reticulum homeostasis and calcium mobilization in T lymphocytes. *J Immunol* **186**, 1564–1574.
[58] Benbrook DM and Long A (2012). Integration of autophagy, proteasomal degradation, unfolded protein response and apoptosis. *Exp Oncol* **34**, 286–297.
[59] Deegan S, Saveljeva S, Gorman AM, and Samali A (2012). Stress-induced self-cannibalism: on the regulation of autophagy by endoplasmic reticulum stress. *Cell Mol Life Sci*.
[60] Woehlbier U and Hetz C (2011). Modulating stress responses by the UPRosome: a matter of life and death. *Trends Biochem Sci* **36**, 329–337.
[61] Gandesiri M, Chakilam S, Ivanovska J, Benderska N, Ocker M, Di Fazio P, Feoktistova M, Gali-Muhtasib H, Rave-Frank M, Prante O, et al. (2012). DAPK plays an important role in panobinostat-induced autophagy and commits cells to apoptosis under autophagy deficient conditions. *Apoptosis* **17**, 1300–1315.
[62] Bartoszewski R, Brewer JW, Rab A, Crossman DK, Bartoszewska S, Kapoor N, Fuller C, Collawn JF, and Bebok Z (2011). The unfolded protein response (UPR)-activated transcription factor X-box-binding protein 1 (XBP1) induces microRNA-346 expression that targets the human antigen peptide transporter 1 (TAP1) mRNA and governs immune regulatory genes. *J Biol Chem* **286**, 41862–41870.
[63] Behrman S, Acosta-Alvear D, and Walter P (2011). A CHOP-regulated microRNA controls rhodopsin expression. *J Cell Biol* **192**, 919–927.
[64] Duan Q, Wang X, Gong W, Ni L, Chen C, He X, Chen F, Yang L, Wang P, and Wang DW (2012). ER stress negatively modulates the expression of the miR-199a/214 cluster to regulates tumor survival and progression in human hepatocellular cancer. *PLoS One* **7**, e31518.
[65] Sampath D, Liu C, Vasan K, Sulda M, Puduvalli VK, Wierda WG, and Keating MJ (2012). Histone deacetylases mediate the silencing of miR-15a, miR-16, and miR-29b in chronic lymphocytic leukemia. *Blood* **119**, 1162–1172.
[66] Rhodes LV, Nitschke AM, Segar HC, Martin EC, Driver JL, Elliott S, Nam SY, Li M, Nephew KP, Burow ME, et al. (2012). The histone deacetylase inhibitor trichostatin A alters microRNA expression profiles in apoptosis-resistant breast cancer cells. *Oncol Rep* **27**, 10–16.
[67] Lee EM, Shin S, Cha HJ, Yoon Y, Bae S, Jung JH, Lee SM, Lee SJ, Park IC, Jin YW, et al. (2009). Suberoylanilide hydroxamic acid (SAHA) changes microRNA expression profiles in A549 human non-small cell lung cancer cells. *Int J Mol Med* **24**, 45–50.

Supplementary Materials and Methods

Real-time Cell Viability Analysis after Panobinostat and Thapsigargin Treatment

The xCELLigence RTCA SP System (Roche Applied Science) was used for real-time and time-dependent analysis of the cellular response of HepG2 and Hep3B cells following incubation with 0.1 μM panobinostat and thapsigargin (10 nM, 100 nM, 1 μM, and 10 μM), as previously described in Materials and Methods section.

Cytosolic and Nuclear Protein Extraction

Cytosolic and nuclear protein fractions were obtained from HepG2 and Hep3B cells after 6 to 72 hours of treatment with 0.1 μM panobinostat and after 24 hours of treatment with 10 nM thapsigargin, by using NP-40 lysis buffer [10 mM Tris-HCl, (pH 7.4), 10 mM NaCl, 3 mM $MgCl_2$, 0.5% (vol/vol) NP-40, protease inhibitors (Roche Applied Sciences)], and with 0.5% Triton X-100 lysis buffer containing 10 mM Tris-HCl, 5 mM $MgCl_2$, and 0.25 M sucrose, performing the previously described protocol [1].

Western Blot Analysis

Whole-cell lysates and cytosolic and nuclear protein fractions were processed by sodium dodecyl sulfate–polyacrylamide gel electrophoresis followed by Western blot analysis, as previously described [1]. Immunodetection applying primary antibodies against IRE1α, S724-IRE1α, ATF4, CHOP (Abcam), histone H3 (Active Motif, La Hulpe, Belgium) as nuclear positive control, and β-actin (Sigma-Aldrich) as cytosolic positive control was performed. Bound secondary HRP-conjugated antibodies (Sigma-Aldrich) were detected by incubating the immunoblots with SuperSignal West Pico Chemiluminescent Substrate (Pierce, Thermo Fisher Scientific). The luminescent reactivity was measured using Fusion image capture and further quantified with Bio1D Analysis System (PEQLAB Biotechnologie GmbH). Anti–histone H3 and anti–β-actin were used to control equal loading and protein quality.

Supplementary Results

Effects of ER Stress Inducer Thapsigargin on HCC Proliferation

Thapsigargin concentration was chosen using impedance-based real-time cell viability analysis with the xCELLigence System (Figure W1, *C* and *D*). These results confirmed previously published data [2] referring to panobinostat effects in HepG2 (Figure W1*C*) and Hep3B (Figure W1*D*) cell lines. Panobinostat (0.1 μM) significantly reduced the normalized cell index in both cell lines and its effect was comparable to 10 nM thapsigargin treatment, the concentration that was adopted for the other experiments.

Panobinostat and Thapsigargin Effects on IRE1α Protein Level Analyzed by Western Blot

IRE1α and its phosphorylated form S724-IRE1α showed an increase after panobinostat treatment in HepG2, in particular after 48 hours, whereas stable levels were detectable in Hep3B cells (Figure W3*B*). Thapsigargin treatment induced IRE1α and S724-IRE1α increase in both cell lines.

Supplementary References

[1] Di Fazio P, Montalbano R, Neureiter D, Alinger B, Schmidt A, Merkel AL, Quint K, and Ocker M (2012). Downregulation of HMGA2 by the pan-deacetylase inhibitor panobinostat is dependent on hsa-let-7b expression in liver cancer cell lines. *Exp Cell Res* **318**, 1832–1843.

[2] Di Fazio P, Schneider-Stock R, Neureiter D, Okamoto K, Wissniowski T, Gahr S, Quint K, Meissnitzer M, Alinger B, Montalbano R, et al. (2010). The pan-deacetylase inhibitor panobinostat inhibits growth of hepatocellular carcinoma models by alternative pathways of apoptosis. *Cell Oncol* **32**, 285–300.

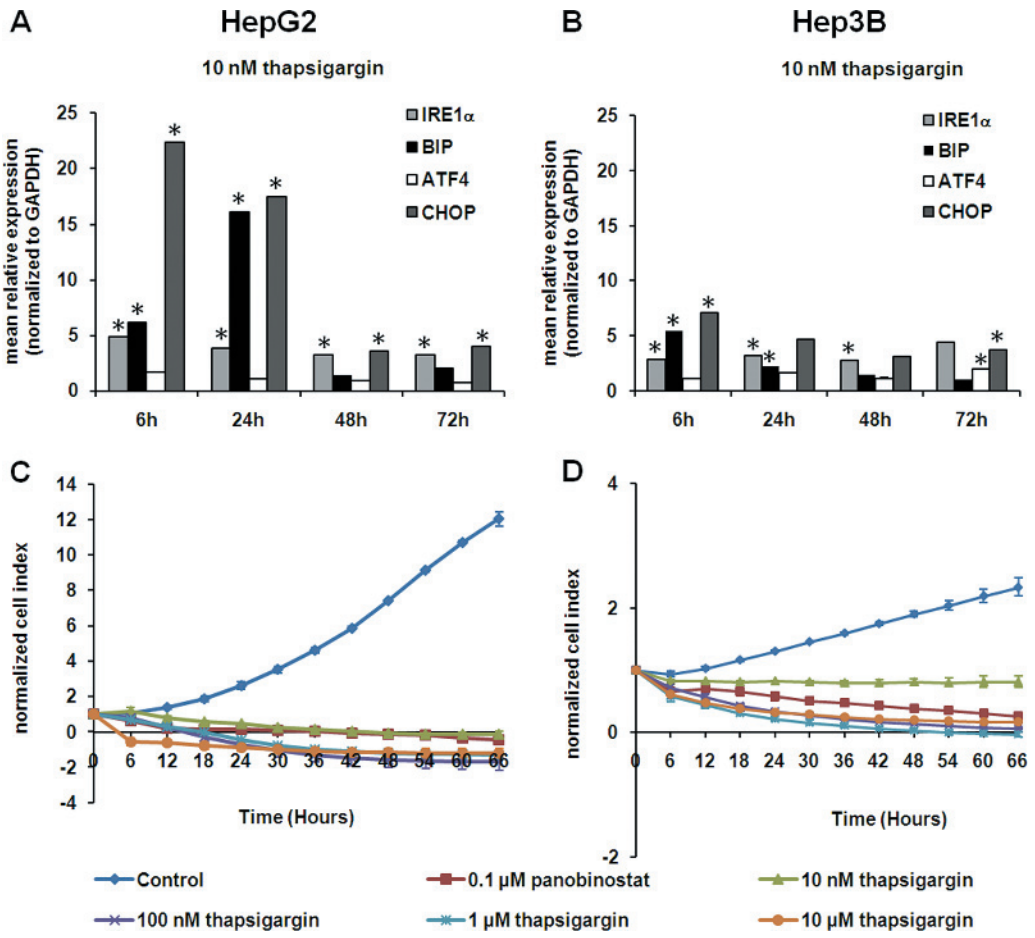

Figure W1. Comparison between panobinostat and thapsigargin effects. Quantitative real-time RT-PCR analysis after 6, 24, 48, and 72 hours of treatment with 10 nM thapsigargin in HepG2 (A) and Hep3B (B) cells showing an increase of IRE1α, BiP, ATF4, and CHOP. mRNA expression was normalized to GAPDH and results are expressed relative to untreated controls set at 1.0. Means ± SD of three independent experiments performed in triplicates are shown. *$P < .05$ *versus* control. For the impedance-based real-time cell viability study, HepG2 (C) and Hep3B (D) cells were cultured in E-plates and treated with 0.1 μM panobinostat and different concentrations of thapsigargin (10 nM–10 μM). Cell index was normalized to the time point of treatment. Cell index was determined continuously for additional 70 hours. Means ± SD of three independent experiments performed in triplicates are shown.

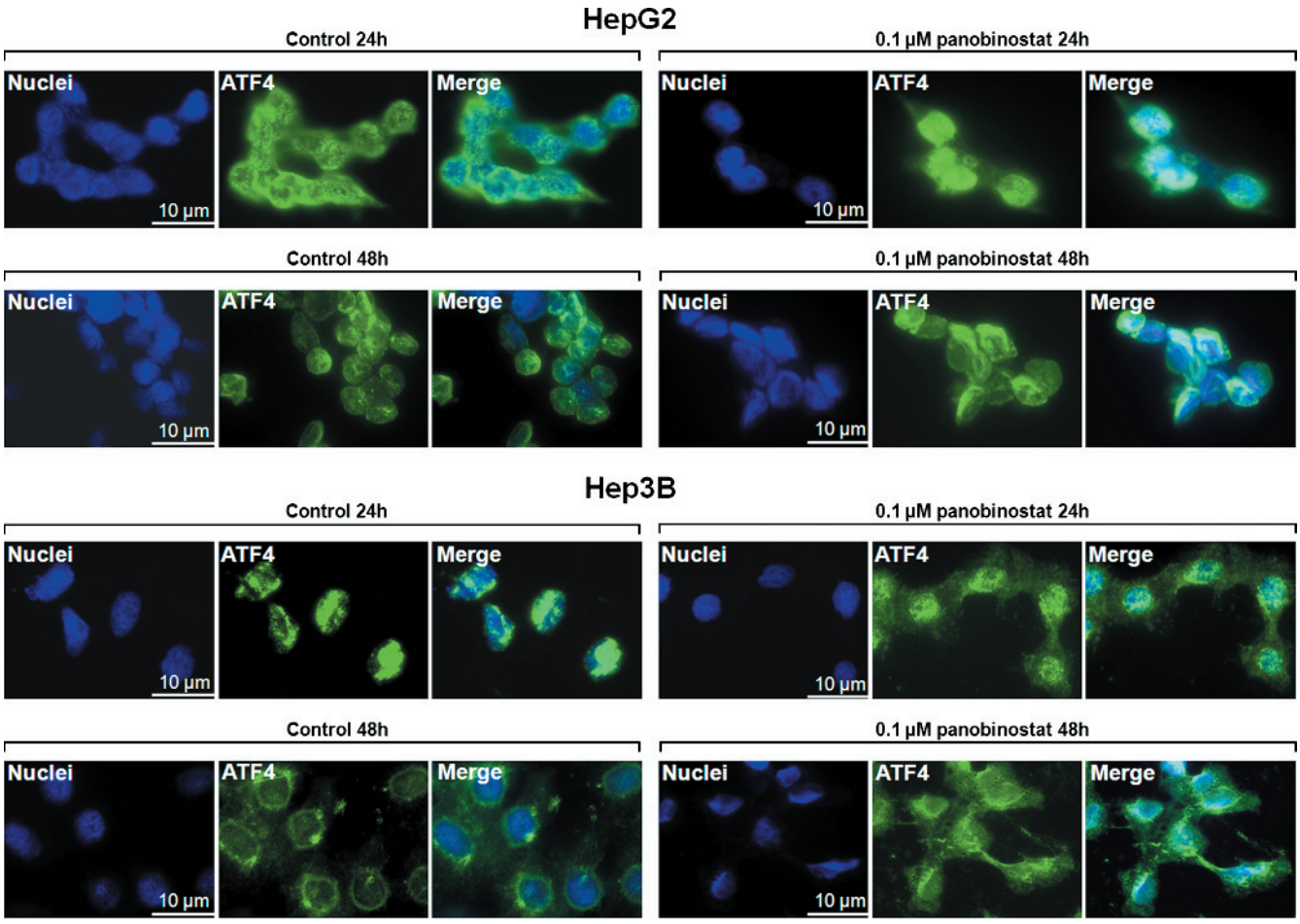

Figure W2. Immunofluorescence analysis of ATF4. The immunofluorescence images in Figure 3*B* are displayed in separated blue, green, and merged panels (from left to right) to present ATF4 nuclear translocation after panobinostat treatment in HepG2 and Hep3B cells. The experiments were performed in triplicates under the same settings.

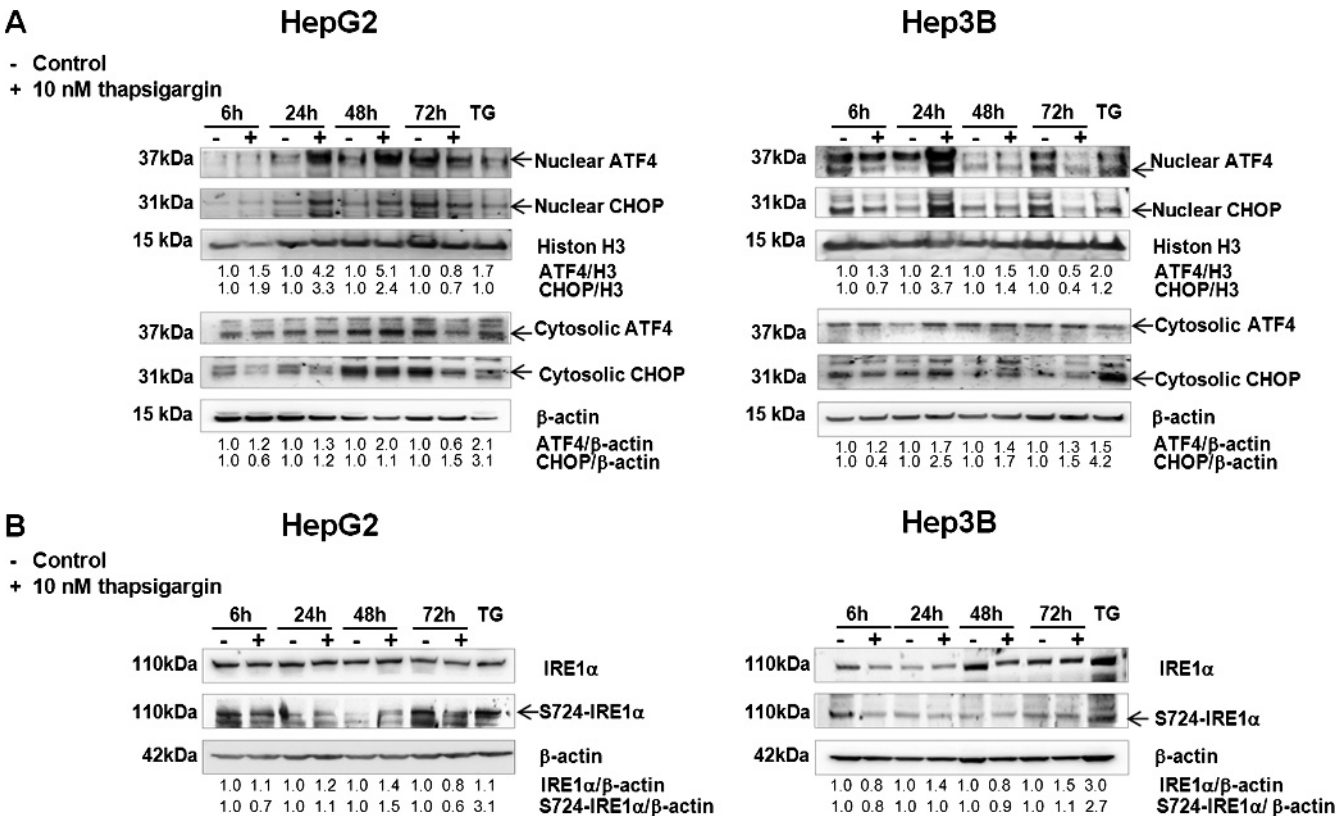

Figure W3. Western blot analysis of ER stress markers. ATF4 and CHOP protein levels (A) were evaluated after 72 hours of treatment with 0.1 μM panobinostat and after 24 hours of treatment with 10 nM thapsigargin in HepG2 (left) and Hep3B (right) cell lines, in nuclear and cytosolic fractions, using histone H3 and β-actin levels as nuclear and cytosolic loading controls, respectively. Arrows indicate the specific bands for ATF4 and CHOP. Densitometry results were normalized to histone H3 and β-actin contents and are expressed relative to untreated controls set at 1.0. IRE1α and S724-IRE1α (B) were evaluated after 72 hours of treatment with 0.1 μM panobinostat and after 24 hours of treatment with 10 nM thapsigargin in HepG2 (left) and Hep3B (right) cell lines in whole-cell lysates. The arrow indicates the specific band for S724-IRE1α. Densitometry results were normalized to β-actin content and are expressed relative to untreated controls set at 1.0. Experiments were performed in triplicates.

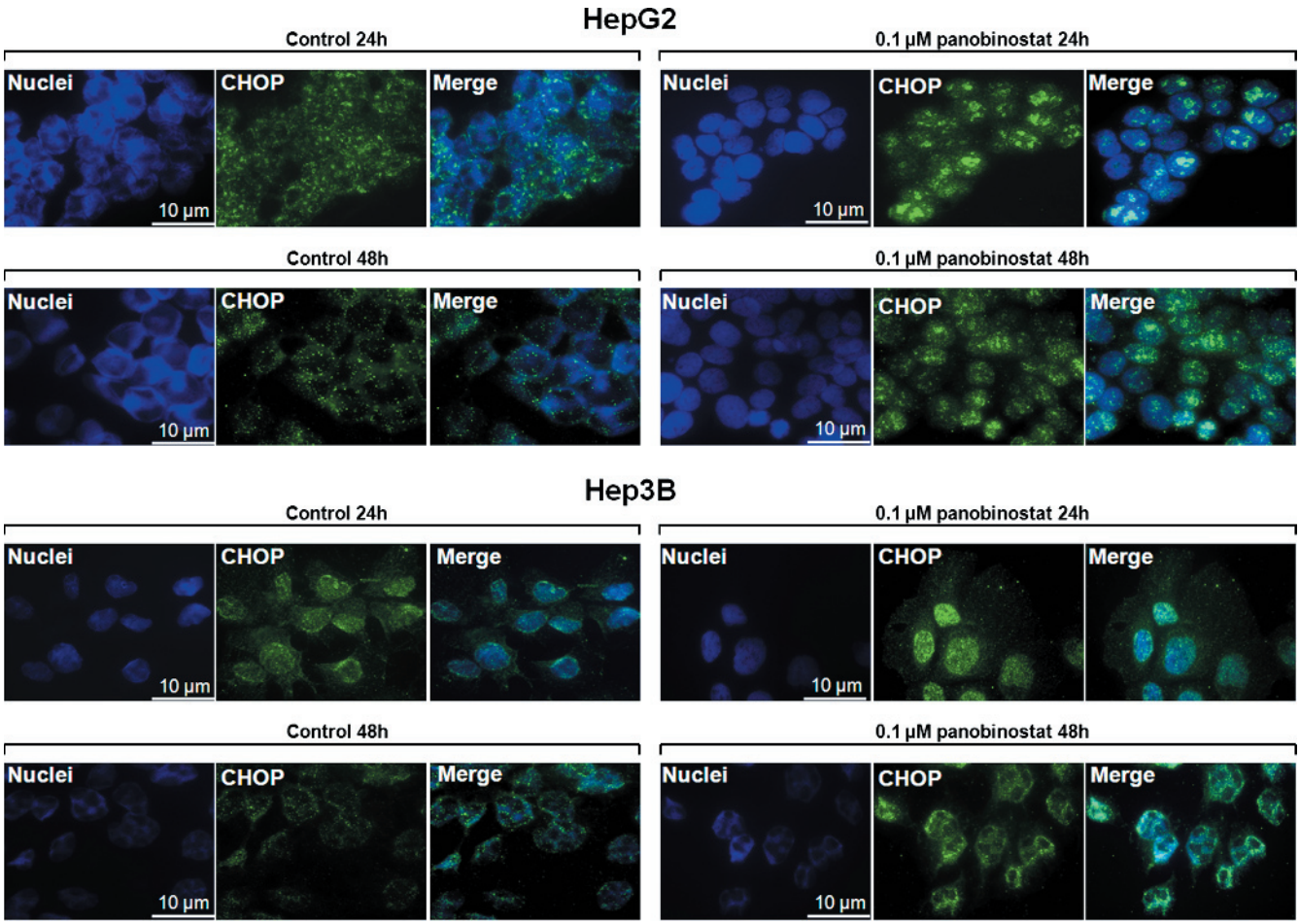

Figure W4. Immunofluorescence analysis of CHOP. The immunofluorescence images of Figure 5*A* are displayed in separated blue, green, and merged panels (from left to right) to present CHOP nuclear translocation after panobinostat and thapsigargin treatment. Experiments were performed in triplicates under the same settings.